Improved cirrus simulations in a general circulation model using CARMA sectional microphysics

C. G. Bardeen, A. Gettelman, E. J. Jensen, A. Heymsfield, A. J. Conley, Julien Delanoë, M. Deng, O. B. Toon

Improved cirrus simulations in a general circulation model using CARMA sectional microphysics

C. G. Bardeen,[1] A. Gettelman,[1] E. J. Jensen,[2] A. Heymsfield,[1] A. J. Conley,[1] J. Delanoë,[3] M. Deng,[4] and O. B. Toon[5]

Received 13 May 2013; revised 30 September 2013; accepted 2 October 2013; published 21 October 2013.

[1] We have developed a new cirrus model incorporating sectional ice microphysics from the Community Aerosol and Radiation Model for Atmospheres (CARMA) in the latest version of NCAR's Community Atmosphere Model (CAM5). Comparisons with DARDAR and 2C-ICE show that CAM5/CARMA improves cloud fraction, ice water content, and ice water path compared to the standard CAM5. Prognostic snow in CAM5/CARMA increases overall ice mass and results in a melting layer at ~4 km in the tropics that is largely absent in CAM5. Subgrid scale supersaturation following Wilson and Ballard (1999) improves ice mass and relative humidity. Increased middle and upper tropospheric condensate in CAM5/CARMA requires a reduction in low-level cloud for energy balance, resulting in a 3.1 W m^{-2} improvement in shortwave cloud forcing and a 3.8 W m^{-2} improvement in downwelling shortwave flux at the surface compared to CAM5 and Clouds and Earth's Radiant Energy Systems (CERES). Total and clear-sky longwave upwelling flux at the top are improved in CAM5/CARMA by 1.0 and 2.6 W m^{-2}, respectively. CAM has a 2–3 K cold bias at the tropical tropopause mostly from the prescribed ozone file. Correction of the prescribed ozone or nudging the CAM5/CARMA model to GEOS5-DAS meteorology yields tropical tropopause temperatures and water vapor that agree with the Constellation Observing System for Meteorology, Ionosphere, and Climate (COSMIC) and the Microwave Limb Sounder (MLS). CAM5 relative humidity appears to be too large resulting in a +1.5 ppmv water vapor bias at the tropical tropopause when using GEOS5-DAS meteorology. In CAM5/CARMA, 75% of the cloud ice mass originates from ice particles detrained from convection compared to 25% from in situ nucleation.

Citation: Bardeen, C. G., A. Gettelman, E. J. Jensen, A. Heymsfield, A. J. Conley, J. Delanoë, M. Deng, and O. B. Toon (2013), Improved cirrus simulations in a general circulation model using CARMA sectional microphysics, *J. Geophys. Res. Atmos.*, *118*, 11,679–11,697, doi:10.1002/2013JD020193.

1. Introduction

[2] Ice clouds are an important part of the Earth's climate system, providing a significant radiative forcing [*Liou*, 1986; *Comstock et al.*, 2002], participating in the dehydration of air entering the stratosphere [*Jensen et al.*, 1996; *Jensen et al.*, 2007], and playing a role in troposphere-stratosphere exchange [*Corti et al.*, 2006]. Use of general circulation models (GCMs) to evaluate the role of ice clouds in the climate system is complicated by the wide range of results for cirrus ice water content (IWC) from these models [*Waliser et al.*, 2009]. In part, these differences are because cloud processes typically occur on smaller spatial and temporal scales than that of a climate model and also because cirrus microphysical and resulting radiative properties have traditionally been poorly constrained by data. Smaller scales necessitate the development of subgrid scale parameterizations for cloud processes. *Gettelman and Birner* [2007] indicate that for these reasons, cirrus are likely to be the source of the most uncertainty in simulations of the tropical tropopause layer (TTL).

[3] Cirrus in the upper troposphere and lower stratosphere (UTLS) can result from outflow from convective clouds or by in situ ice nucleation [*Pfister et al.*, 2001]. Occasionally, deep convection can penetrate the stratosphere [*Danielsen*, 1993; *de Reus et al.*, 2009], providing a direct injection of ice and water. The microphysical and optical properties of cirrus clouds are affected by the conditions under which they are formed, and these properties in turn affect dehydration of air parcels prior to entering the stratosphere. Current models do a good job of reproducing the large-scale structure of the TTL [*Gettelman et al.*, 2010a] but have trouble simulating the cold-point temperature, stratospheric water vapor, cloud fraction, and ozone [*Randel and Jensen*, 2013].

[1]National Center for Atmospheric Research, Boulder, Colorado, USA.
[2]NASA Ames Research Center, Moffett Field, California, USA.
[3]LATMOS, UVSQ/CNRS, IPSL, Guyancourt, France.
[4]University of Wyoming, Laramie, Wyoming, USA.
[5]Department of Atmospheric and Oceanic Sciences and Laboratory for Atmospheric and Space Physics, Boulder, Colorado, USA.

Corresponding author: C. G. Bardeen, National Center for Atmospheric Research, PO Box 3000, Boulder, Colorado, 80307-3000, USA. (bardeenc@ucar.edu)

2169-897X/13/10.1002/2013JD020193

[4] Observations inside of cirrus are complicated by their remoteness and by the wide range of ice crystal sizes, shapes, and optical depths [*Comstock et al*., 2006]. Past in situ microphysical observations have also been affected by ice particle shattering by the probes used to sample them [*Heymsfield*, 2007; *Lawson*, 2011; *Korolev et al*., 2011]. Ice in the mixed-phase temperature range (0°C to −40°C) is particularly hard to characterize because of the presence of both water drops and ice particles complicating the retrievals [*Korolev et al*., 2003]. The 2006 launch of the CloudSat [*Stephens et al*., 2008] and Cloud-Aerosol Lidar and Infrared Pathfinder Satellite Observation (CALIPSO) [*Winker et al*., 2009] satellites provide space-based radar and lidar observations of clouds and offer exciting new data sets with which to constrain the models. Recently, joint retrievals of ice cloud properties using both CloudSat and CALIPSO data and optimal estimation techniques [*Deng et al*., 2010; *Delanoë and Hogan*, 2010; *Delanoë and Hogan*, 2008] have provided seamless data sets extending from the thin ice clouds in the UTLS to optically thick clouds in convective regions.

[5] The availability of these new data sets with vertically resolved IWC based upon CloudSat, CALIPSO, and the combination of the two have motivated several broad multimodel intercomparisons of cloud properties [*Waliser et al*., 2009; *Chen et al*., 2011; *Li et al*., 2012; *Jiang et al*., 2012] as well as more in-depth comparisons with individual models [*Gettelman et al*., 2010b; *Delanoë et al*., 2011; *Song et al*., 2012]. Multimodel comparisons show a wide range of IWC values from the models, with differences of as much as a factor of 2 to 10 in ice water path (IWP) compared with uncertainties in the observations of about a factor of 2 [*Li et al*., 2012]. Difficulties in the analysis include deciding how to deal with the mixture of cloud ice with convective and precipitating condensate in the observations that may not be reported by all models [*Waliser et al*., 2009]. Improvements have been seen between the Coupled Model Intercomparison Project Phase 3 and Phase 5 models with a ~50% reduction in the IWP multimodel mean bias [*Li et al*., 2012]; however, no significant improvement is seen for water vapor [*Jiang et al*., 2012]. The comparisons to individual models are often done to evaluate changes to the model's parameterizations. In *Delanoë et al*. [2011], improvements were seen by using prognostic instead of diagnostic precipitation, while *Gettelman et al*. [2010b] showed improvements by using two-moment stratiform cloud microphysics and by allowing water vapor supersaturation with respect to ice. *Song et al*. [2012] achieved improved IWC by replacing the bulk cloud microphysics in the convection parameterization with a two-moment scheme.

[6] Using the new CloudSat- and CALIPSO-based cirrus data sets, we characterize the representation of cirrus within the most recent versions of the Community Atmosphere Model (CAM) [*Neale et al*., 2010a; *Neale et al*., 2010b] and explore whether changes to the ice microphysics and related parameterizations in this model can improve the global representation of cirrus clouds and also have an impact on temperature and water vapor in the TTL. In our new model, CAM5/CARMA, we replace the two-moment CAM5 stratiform ice microphysics with sectional microphysics from the Community Aerosol and Radiation Model for Atmospheres (CARMA) version 3.0 (Bardeen et al., in preparation). The formulation of the model is described in section 2. Section 3 contains results of several simulations that are compared with each other and also with observations of clouds, temperature, and water vapor. Finally, a discussion of the results and summary of the major conclusions are presented in section 4.

2. Model Description

[7] This study uses versions 4 and 5 of the Community Atmosphere Model [*Neale et al*., 2010a; *Neale et al*., 2010b], the atmospheric model component of the Community Earth System Model [*Hurrell et al*., 2013]. CAM4 uses a bulk parameterization for stratiform clouds [*Rasch and Kristjansson*, 1998] where water vapor, liquid cloud mass, and ice cloud mass are prognosed. CAM5 utilizes the Morrison-Gettelman two-moment microphysics [*Morrison and Gettelman*, 2008; *Gettelman et al*., 2010b], which adds prognostic liquid and ice cloud particle concentration. CAM5 allows for water vapor to be supersaturated with respect to ice, which was not allowed in CAM4. CAM4 and CAM5 both diagnose rain and snow. We extend CAM5 by replacing the two-moment stratiform ice microphysics with sectional microphysics using version 3.0 of the Community Aerosol and Radiation Model for Atmospheres (Bardeen et al., in preparation) and provide a prognostic treatment for snow. All experiments use prescribed bulk aerosols to eliminate radiative differences caused by changes in aerosol loading.

2.1. CAM5/CARMA

[8] CARMA is an extensible microphysics package that allows for a size-resolved treatment of aerosols and clouds and is available as an optional component within CAM5 [*Bardeen et al*., 2008]. Figure 1 shows the microphysical particle types and processes that are treated by the CAM5/CARMA cirrus model. It uses a prescribed sulfate aerosol from an independent Whole Atmosphere Community Climate Model with CARMA microphyscs (WACCM/CARMA) simulation [*English et al*., 2011], a sectional representation of the two-moment cloud liquid and two different types of ice particles: in situ and detrained. Neither the sulfate aerosol bins nor the liquid bins are advected by CAM. Since the sulfates are prescribed, they do not need to be advected. Most of the liquid microphysics is done in the two-moment parameterization, except for the Bergeron-Findeisen process, melting of ice particles at temperatures greater than 0°C and freezing of liquid drops at temperature less than −40°C, which is handled by CARMA. To accomplish this, for each model time step the two-moment representation for cloud drops is converted to a size distribution using the gamma distribution assumed by the two-moment microphysics [*Morrison and Gettelman*, 2008] for CARMA processing, and the results are then converted back into the total liquid mass and the total liquid number for CAM processing. It is the two-moment representation of liquid clouds that is advected. For ice clouds the individual components of the CARMA bin representation are advected. The in situ ice particles are formed by homogeneous freezing of sulfate particles in CARMA, and detrained ice comes from the CAM5 convective parameterizations. For simplicity, we have left out heterogeneous nucleation in the initial version of the model. Results from *Gettelman et al*. [2012] with the CAM5 model indicate that homogeneous freezing is the most important nucleation process, and we expect sulfate aerosols to be

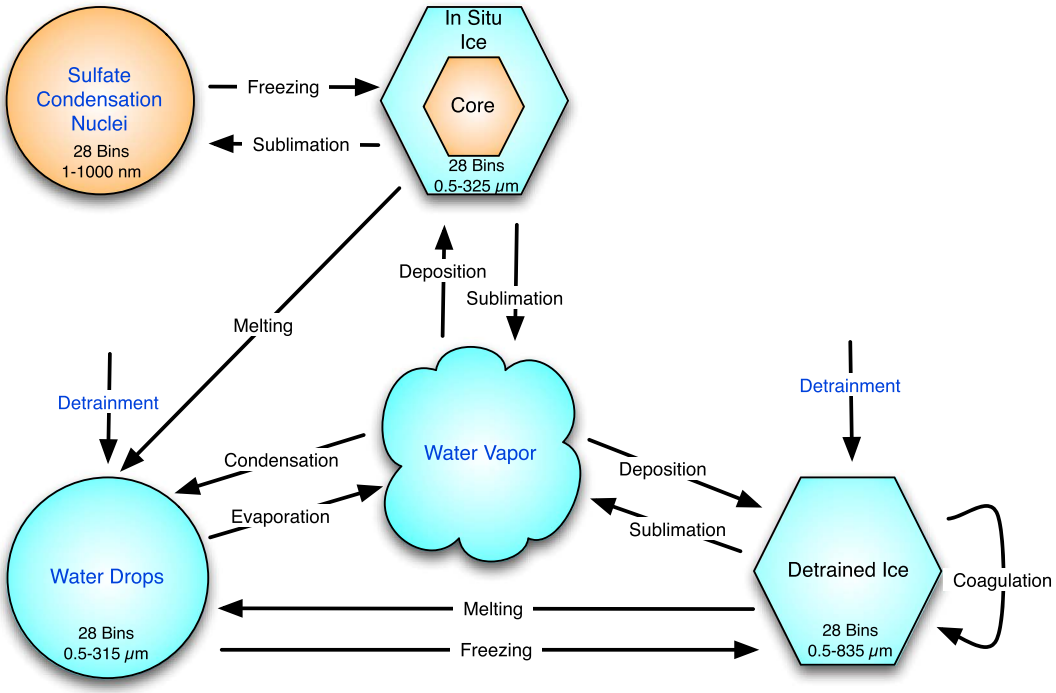

Figure 1. The CARMA microphysical model used with the CAM5/CARMA model. In situ and detrained ice particles are advected as size bins (black labels), while sulfate nuclei are prescribed and water drops are converted to/from their two-moment representation (blue labels). Water vapor is fully interactive, and detrained condensate comes from the convective parameterizations.

much more plentiful than ice nuclei. Ice particle mass, ice number, and ice effective radius are calculated from CARMA, allowing the standard interface to the CAM5 radiation code to be used. Most "snow" is prognosed within the sectional microphysics and is treated as large ice particles, although some diagnostic snow can be created in the two-moment microphysics by the freezing of raindrops. All processes that modify cloud ice have been disabled in the two-moment microphysics, since this is being handled by CARMA. Several of the CAM5 parameterizations have been changed for CAM5/CARMA as described in the following sections. For those not interested in the details of the CAM model changes, please skip ahead to either section 2.2 where the CARMA model changes are described or to section 3 where the results are presented.

2.1.1. Vapor Pressure

[9] For increased accuracy at low temperatures and consistency between CAM and CARMA microphysics, the vapor pressure of water over ice and liquid is calculated by using the *Murphy and Koop* [2005] parameterization rather than the *Goff and Gratch* [1946] parameterization previously used in CAM.

2.1.2. Cloud Fraction and Subgrid Scale Saturation

[10] Ice clouds typically do not fill the entire $1.9° \times 2.5°$ model grid box, so a cloud fraction is necessary. For nucleation and growth to occur within a subset of the grid box, it is further assumed that the water vapor is not homogenously distributed. For CAM5/CARMA, the ice cloud fraction and subgrid scale ice supersaturation from *Wilson and Ballard* [1999] are used. The ice cloud fraction is used by both CAM and CARMA, while the subgrid scale supersaturation is only used by CARMA. The total cloud fraction, combining the ice and liquid cloud fractions, is done the standard way in CAM5 assuming no overlap between the ice and liquid regions.

[11] In *Wilson and Ballard* [1999], the ice cloud fraction ($\mathrm{cf_{ice}}$) is determined by

$$\begin{aligned} \mathrm{cf_{ice}} &= 0 && n_{\mathrm{cf}} \le 0 \\ \mathrm{cf_{ice}} &= 0.5\,(6n_{\mathrm{cf}})^{2/3} && 0 < n_{\mathrm{cf}} \le \frac{1}{6} \\ \mathrm{cf_{ice}} &= 1 - 4\cos^2(\phi) && \frac{1}{6} < n_{\mathrm{cf}} < 1 \\ \mathrm{cf_{ice}} &= 1 && n_{\mathrm{cf}} \ge 1 \end{aligned} \tag{1}$$

where

$$n_{\mathrm{cf}} = \frac{q_{\mathrm{ice}}}{\left[(1 - \mathrm{RH_{crit}})q_{\mathrm{sat,liq}}\right]} \tag{2}$$

$$\phi = \left[\cos^{-1}\left\{\frac{3(1 - n_{\mathrm{cf}})}{2^{\frac{3}{2}}}\right\} + 4\pi\right]/3 \tag{3}$$

q_{ice} is the cloud ice mixing ratio, $q_{\mathrm{sat,liq}}$ is the saturation mixing ratio with respect to liquid, and $\mathrm{RH_{crit}}$ is the critical relative humidity for ice cloud formation. n_{cf} represents the fraction of the maximum possible cloud ice that is present, assuming that at $q_{\mathrm{sat,liq}}$ liquid cloud would start to form. Sensitivity tests of CAM5/CARMA with different $\mathrm{RH_{crit}}$ values (not shown) indicate that a value for $\mathrm{RH_{crit}}$ of 0.7 gives a zonal average cloud fraction in the tropics that is similar to CloudSat/CALIPSO observations.

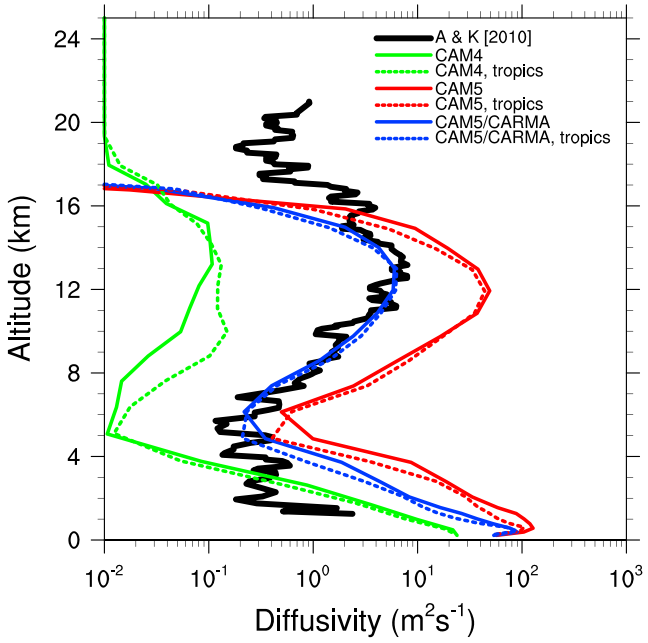

Figure 2. Annual average vertical diffusivity from CAM4, CAM5, and CAM5/CARMA for the tropics (dotted) and for the Bay of Bengal and Arabian Sea (solid) compared to observations from *Alappattu and Kunhikrishnan* [2010] in the Bay of Bengal and Arabian Sea.

[12] The subgrid scale supersaturation for liquid (S_{liq}) and ice (S_{ice}) used by CARMA for nucleation and growth is then determined by:

$$S_{\mathrm{liq}} = \left(q - \alpha q_{\mathrm{sat,liq}}\right)/q_{\mathrm{sat,liq}} \tag{4}$$

$$S_{\mathrm{ice}} = \left(q - \alpha q_{\mathrm{sat,ice}}\right)/q_{\mathrm{sat,ice}} \tag{5}$$

where

$$\alpha = \mathrm{RH_{crit}}(1 - \mathrm{cf}) + \mathrm{cf} \tag{6}$$

q is the water vapor mixing ratio, $q_{\mathrm{sat,ice}}$ is the saturation mixing ratio with respect to ice, and cf is the overall cloud fraction. Supersaturation with respect to ice is allowed [*Gettelman et al.*, 2010b], but both grid- and subgrid-scale supersaturation is limited so that there is no supersaturation with respect to liquid. Because of the different middle and high cloud distributions in CAM5/CARMA, preservation of top of atmosphere radiative balance requires a change in the low cloud fraction, with a value of 0.96 used for the critical relative humidity for the formation of low clouds (RHMINL) instead of 0.8875 that was used in CAM5. All cloud microphysics in both CAM and CARMA is done using in-cloud concentrations determined by scaling the advected grid-box average condensate values with the cloud fraction.

2.1.3. Convective Detrainment

[13] The CAM5 bulk convective parameterizations determine the mass of condensate detrained by convection but do not specify the condensate phase or the particle sizes. In the CAM macrophysics, a linear ramp of phase with temperature is assumed. When the temperature is less than −20°C, all detrained condensate is assumed to be ice; when the temperature is greater than 0°C, all detrained condensate is assumed to be liquid; and between these temperatures a linear combination of ice and liquid is assumed. In CAM5, the ice particle radius is assumed to be 50 μm for detrainment from shallow convection and 25 μm from deep convection. The liquid particle sizes are 10 μm from shallow convection and 8 μm from deep convection. In CAM5/CARMA, the same linear ramp is used for the condensate phase; however, the ice particles are detrained as a temperature-dependent size distribution. The size distribution is based upon *Heymsfield et al.* [2010]:

$$dN = N_0 \mathrm{e}^{-\lambda D} \tag{7}$$

where

$$\lambda = \alpha e^{\beta T} \tag{8}$$

[14] D is the maximum diameter in centimeters, temperature is in Celsius, and α and β are chosen based upon a fit to convective clouds and are 2.425 cm^{-1} and −0.088 C^{-1}, respectively. *Heymsfield et al.* [2010] limit the temperature to −60°C; however, we extended use of this parameterization to colder temperatures. For liquid particles, a size of 8 μm is assumed.

2.1.4. Prognostic Snow

[15] In CAM4 and CAM5, snow is diagnosed by the microphysics code, mostly based upon the autoconversion of ice to snow. In CAM5, autoconversion of ice to snow occurs when ice particles reach a diameter of 400 μm. CAM4 uses a critical mass mixing ratio, since size is not prognosed. It is then assumed that any snow diagnosed by the model will fall to the ground within one time step and all diagnosed snow is removed from the atmosphere before the next time step. For CAM5/CARMA, "snow" is prognostic and the size bins for ice have been extended to large particle sizes, so there is no autoconversion of ice to snow and no assumption about how long it will take for large ice particles to sediment to the ground. CARMA calculates sedimentation velocities for each size bin and ice remains until it has fallen all the way to the surface. In CAM5/CARMA, some "snow" can still be diagnosed from the freezing of raindrops, and this snow is removed at the end of the time step.

2.1.5. Vertical Diffusion

[16] CAM uses a vertical diffusion parameterization to represent unresolved turbulent mixing of temperature, momentum, and tracers. In the free atmosphere, the wind shear, the gradient in virtual potential temperature, and a chosen length scale determine the diffusivity. In CAM4, K_h, the vertical diffusivity, is determined by

$$K_h = l_h^2 S F_h(Ri) \tag{9}$$

where l_h is the mixing length, S is the vertical wind shear, F_h is a stability function, and Ri is the Richardson number. In CAM5, the moist turbulence scheme does something similar; however, this time the vertical diffusivity is determined by

$$K_h = l S_h E_{\mathrm{tke}}^{\frac{1}{2}} \tag{10}$$

where l is the dissipation length, S_h is a stability function, and E_{tke} is the diagnosed turbulent kinetic energy. E_{tke} is proportional to l^2, so both the CAM4 and CAM5 schemes have diffusivities that are proportional to the square of the length scale. In CAM4, the length scale in the free troposphere is

fixed at 30 m; however, in CAM5 it is diagnosed from the height of the unstable layer and can get much larger.

[17] As shown in Figure 2, the average vertical diffusivities in CAM5 are several orders of magnitude larger than they were in CAM4 and are larger than observations *Alappattu and Kunhikrishnan* [2010] made using high-resolution radiosondes in the Bay of Bengal and Arabian Sea. In the models, the tropical average diffusivity is very similar to the diffusivity calculated just in the region studied by *Alappattu and Kunhikrishnan* [2010]. Using this increased diffusivity causes CAM5/CARMA to have a tropopause that is too high and too wet. Therefore, in CAM5/CARMA, the diagnosed diffusivity is limited to values similar to *Alappattu and Kunhikrishnan* [2010] by restricting the maximum turbulent length scale calculated in the CAM5 moist turbulence parameterization to 100 m outside of the boundary layer. The inability of any of the models to reproduce the diffusivity seen in the observations from 16 to 19 km suggests that convection or some other source of mixing may not extend high enough in the models in the tropics.

2.2. CARMA

[18] CARMA 3.0 (Bardeen et al., in preparation) has several features that have been enhanced or added since CARMA 2.3 [*Turco et al*., 1979; *Toon et al*., 1988; *Jacobson et al*., 1994] for the cirrus model. These include a new parameterization for homogeneous freezing of aqueous aerosols, variable particle density between bins, a new fall velocity parameterization for ice particles, a retry mechanism for more efficiently substepping the fast microphysics, and more rigorous mass and energy conservation. For those not interested in the details of the changes to the CARMA model, please skip ahead to the results in section 3.

2.2.1. Variable Ice Density

[19] Ice particles in convective clouds may have many sizes and habits. Once they are detrained into the large-scale environment, they may undergo further growth and coagulation. In CARMA, the size bins represent the mass of spherical particles with a certain mean radius. For detrained ice particles, we approximate the effect of various particle habits by using a spherical particle with a reduced density based upon an assumed maximum diameter and projected area. The maximum diameter ($D_{\max}$) and density (ρ_{ice}) are determined by a mass-diameter relationship from observed clouds [*Heymsfield et al*., 2010]:

$$D_{\max} = \sqrt[b]{m/a} \tag{11}$$

$$\rho_{\text{ice}} = \frac{6m}{\pi D_{\max}^3} \tag{12}$$

where m is the mass of the particle in grams, $D_{\max}$ is in centimeters, and a and b are fit parameters. We are using $a = 3.79 \times 10^{-3}$ and $b = 2.1$, which are appropriate for warm clouds. We experimented with fits for different types of clouds and found that using the fit for warm ice clouds matched the observations best and on average may better represent the particle distribution as the detrained particles merge into the large scale.

[20] The area ratio (Ar) is also determined for each size bin. It is the ratio of the projected area of the particle to the area of a circle whose diameter is determined from the maximum diameter using *Schmitt and Heymsfield* [2009]:

$$\begin{aligned} \text{Ar} &= e^{-38 D_{\max}} && D_{\max} \le 200\,\mu\text{m} \\ \text{Ar} &= 0.16 {D_{\max}}^{-0.27} && D_{\max} > 200\,\mu\text{m} \end{aligned} \tag{13}$$

[21] The particle's maximum diameter, area ratio, and density will then control the particle growth, coagulation, and sedimentation as determined by CARMA.

2.2.2. Fall Velocity

[22] CARMA has general-purpose fall velocity routines; however, there are some discontinuities in the fall velocity as you go from one Reynolds number regime to another. For this study, we use the parameterization for ice particle fall velocities from *Heymsfield and Westbrook* [2010]. This parameterization utilizes the mass, maximum diameter, and area ratio that have already been calculated for the ice particles to determine the fall velocity:

$$X^* = \frac{\rho_{\text{air}}}{\eta^2} \frac{8mg}{\pi A_r^{0.5}} \tag{14}$$

$$Re = \frac{\delta_0^2}{4} \left[\left(1 + \frac{4\sqrt{X^*}}{\delta_0^2 \sqrt{C_0}} \right)^{1/2} - 1 \right]^2 \tag{15}$$

$$v_t = \frac{\eta Re}{\rho_{\text{air}} D_{\max}} \tag{16}$$

where $C_0 = 0.35$, $\delta_0 = 8.0$, η is the dynamic viscosity of air (erg s), ρ_{air} is the air density (g cm^{-3}), and g is the acceleration from gravity (cm s^{-2}).

2.2.3. Homogeneous Freezing

[23] CARMA 2.3 includes a parameterization for homogeneous freezing of sulfate aerosols based upon *Tabazadeh et al*. [2000]. For these experiments, we instead use a homogenous freezing parameterization based upon water activity from *Koop et al*. [2000] including the Kelvin effect on small particles.

2.2.4. Retry Mechanism

[24] The timescale for ice nucleation and growth can be much faster than the 30 min time step of the CAM model. CARMA addresses this by substepping the nucleation and growth processing. In the past, in some three-dimensional cloud models using CARMA, the number of substeps had to be set large enough to withstand the fastest time scale that would ever be encountered by the model; otherwise, the model could overshoot and cause the run to fail. In CAM, this fixed substep proved to be unmanageable, so a variable timescale was introduced. The model first makes a guess at the appropriate number of substeps; however, if the solution fails to converge properly, it will start the growth and nucleation step over again doubling the number of substeps, repeating this until the model converges. For this cirrus model, the average number of substeps used per grid box per time step is less than 2, but on occasion 64,000 or more substeps may be needed. This change has made it practical to run the CARMA cirrus model in CAM.

2.2.5. Mass and Energy Conservation

[25] Climate models tend to have rigorous mass and energy conservation requirements since the simulations can last for long periods of time. Drifts in the model due to a lack of mass or energy conservation can cause erroneous results. CARMA implicitly solves the growth and nucleation processes, but explicitly solves for the associated gas concentrations. This

Table 1. Numerical Simulations Used for This Study[a]

	Vertical Levels	Ice Microphysics	Specified Meteorology	Prescribed Ozone
CAM4	24	RK		Standard
CAM5	30	MG		Standard
CAM5 O_3	30	MG		Scaled
SD-CAM5	56	MG	GEOS5.2	Standard
CAM5/CARMA	30	CARMA		Standard
CAM5/CARMA O_3	30	CARMA		Scaled
SD-CAM5/CARMA	56	CARMA	GEOS5.2	Standard

[a]The ice microphysics is either Rasch and Kristjansson (RK), Morrison and Gettelman (MG), or CARMA.

can cause small errors in mass and energy conservation. To achieve conservation, the change in condensable gases and latent heat is calculated by comparing the total condensate before and after the time step. This method results in mass and energy conservation that meets CAM's requirements.

3. Results

[26] Table 1 contains a list of the numerical simulations performed for this study using CAM4, CAM5, and CAM5/CARMA as free-running models and also for the CAM5 models using specified dynamics [*Lamarque et al.*, 2011], where some of the model state is nudged [*Kunz et al.*, 2011] toward meteorology from the Goddard Earth Observing System Model, Version 5 Data Assimilation System (GEOS5-DAS) version 5.2 [*Rienecker et al.*, 2008]. In the specified dynamics runs, the model winds, temperature, specific heat, latent heat, and surface stresses are corrected each time step with 1% of the difference between the assimilated and model values. The assimilated data are available every 6 h, so the values are interpolated for intervening time steps. All other fields are left unconstrained. All simulations are done at $1.9° \times 2.5°$ horizontal resolution and have from 24 to 56 vertical levels with a model top of ~1 hPa. Each simulation is run for 8 years. For most results, the last 5 years of the simulation is used for the analysis. We first look at the ice cloud characteristics from a global perspective and then examine tropical averages of water vapor, temperature, relative humidity, and cloud properties.

3.1. Global Analysis of Cloud Properties

[27] CloudSat [*Stephens et al.*, 2008] and CALIPSO [*Winker et al.*, 2009] are two satellites in the A-Train [*Stephens and Vane*, 2007] that measure ice clouds. The Cloud-Aerosol Lidar with Orthogonal Polarization (CALIOP) [*Winker et al.*, 2009] on the CALIPSO satellite is a lidar that is sensitive to the smaller particles in optically thin clouds but can become totally attenuated and unable to see the lower part of optically thick clouds. CloudSat is a radar instrument that is sensitive to large particles and is able to penetrate the lower levels of a cloud but does not detect the thinner clouds. Combining CloudSat radar and CALIPSO lidar observations provides an unprecedented global view of cloud phase and cloud properties. For this analysis, we use DARDAR [*Delanoë and Hogan*, 2010; *Delanoë and Hogan*, 2008] and 2C-ICE [*Deng et al.*, 2010], two products that retrieve ice cloud properties by using both CALIOP and CloudSat data. We use DARDAR version 2.1.0 data from 2007–2010 and 2C-ICE version 4 data from 2007–2008. One of the differences between the DARDAR and 2C-ICE retrievals is how they determine whether the condensate is ice or liquid. DARDAR assumes that all condensate with a wet-bulb temperature, $T_{wb} < 0°C$

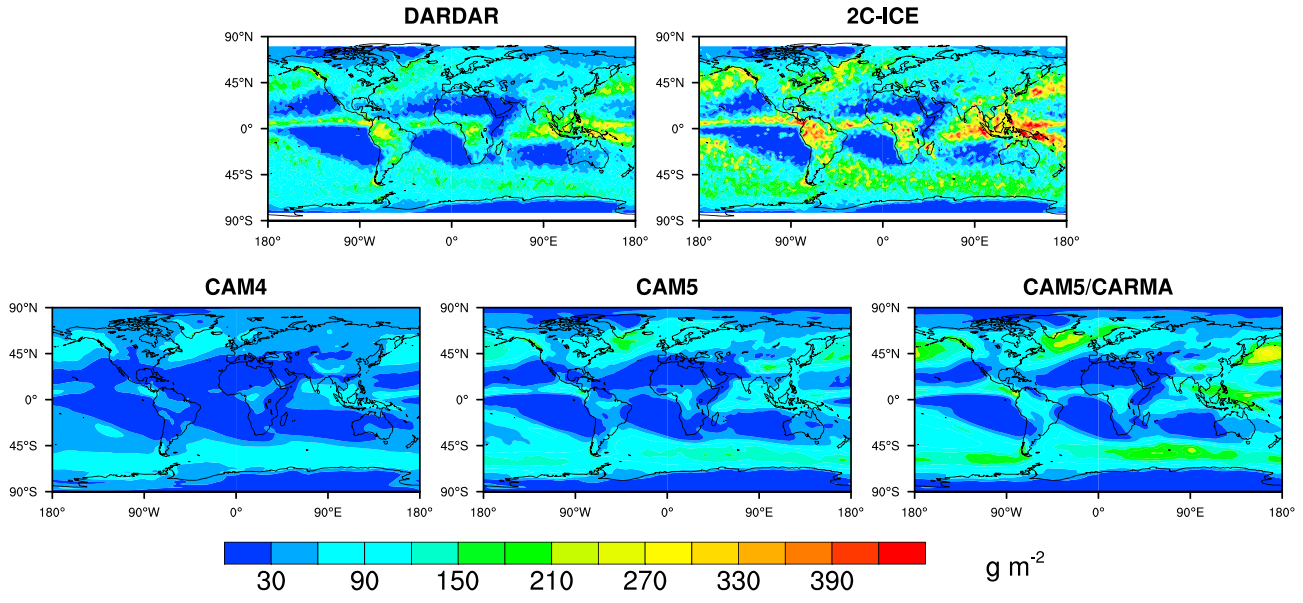

Figure 3. Annual average ice water path for DARDAR (2007–2010), 2C-ICE (2007–2008), and the last 5 years of the CAM4, CAM5, and CAM5/CARMA free-running simulations.

Table 2. Annual Average Global and Tropical Average IWP and the Tropical to Global IWP Ratio From the DARDAR and 2C-ICE and From the Free-Running Models

	Global IWP ($g\,m^{-2}$)	Tropical IWP ($g\,m^{-2}$)	Tropical/ Global
DARDAR	85.7	95.2	1.11
2C-ICE	124.9	144.0	1.15
CAM4	37.0	28.5	0.77
CAM5	55.6	41.9	0.75
CAM5/CARMA	70.9	60.8	0.85

is ice, while 2C-ICE looks for $T < -4$°C or whether the cloud is above the cloud water top from the CloudSat LIDAR_AUX product. Another difference between DARDAR and 2C-ICE is that the DARDAR data use the 60 m vertical grid from the CALIPSO lidar and 2C-ICE uses the 240 m vertical grid from the CloudSat radar. Here we resample the data using a linear ramp of condensate with temperature from 0°C to −10°C for both products while retaining their respective vertical grids, as this seems to remove the large peaks in the IWC near the melting layer likely from water or water-coated ice in the DARDAR data and has an ice height profile that is in better agreement with the model results. At temperatures warmer than 0°C all condensate is assumed to be liquid, temperatures colder than −10°C all condensate is assumed to be ice, and in between the condensate is a linear combination of ice and liquid. This choice of ramp means we have repartitioned the condensate from the observations using the temperatures they provide prior to gridding or averaging the data. However, any of these criteria are somewhat arbitrary and retrieval of ice water content near the mixed-phase region (0°C to −20°C) is somewhat uncertain. Using climatologies of DARDAR and 2C-ICE data sets, we are able to compare ice water path (IWP), cloud fraction (CF), and ice water content (IWC) with results from the CAM simulations over the entire Earth.

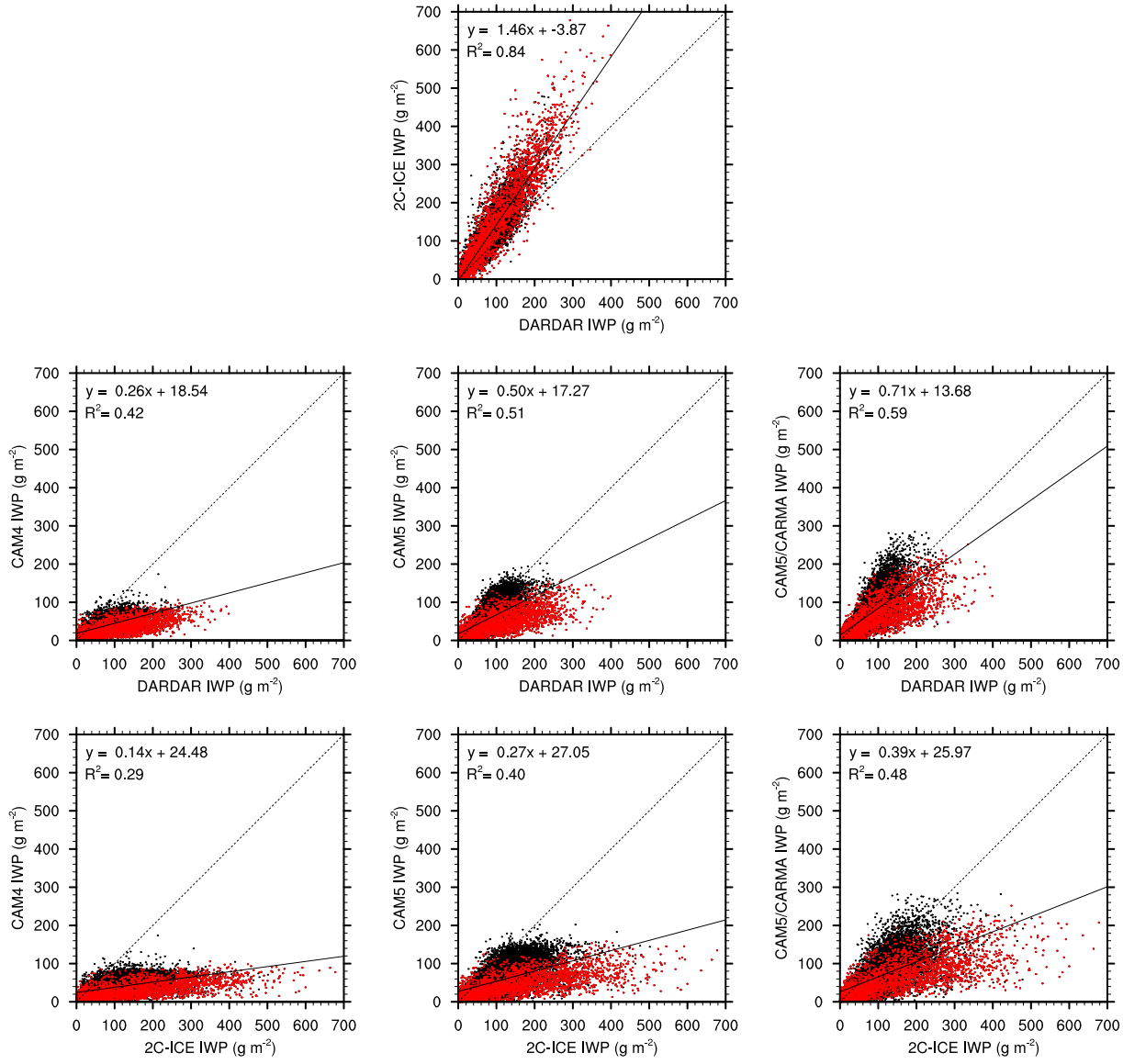

Figure 4. Scatterplots of the annual average IWP for the same data sets as those in Figure 1. Tropical points are in red. Best fits lines to all of the data along with the corresponding R^2 value are shown for each plot.

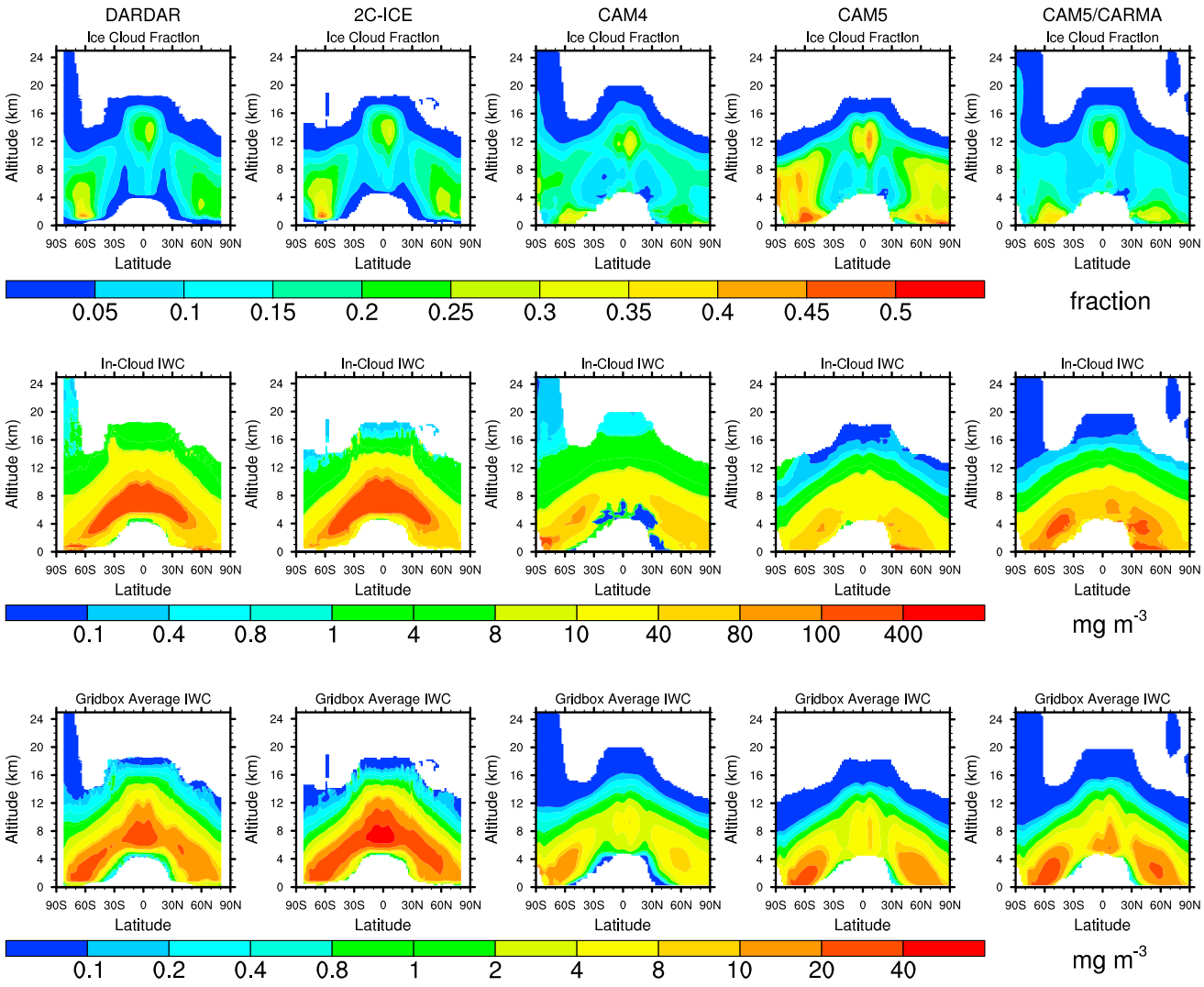

Figure 5. Annual and zonal average cloud fraction, in-cloud ice water content, and grid-box average ice water content for the same data sets as those in Figure 1.

3.1.1. Ice Water Path

[28] Figure 3 shows a map of the annual average ice water path (IWP) from DARDAR, 2C-ICE, and free-running simulations using CAM4, CAM5, and CAM5/CARMA. For all of these simulations, the IWP includes both the cloud ice and any diagnosed snow that is in the atmosphere. All simulations have roughly the same spatial pattern and are in good agreement with the spatial patterns of both observations. In CAM5/CARMA, the IWP in the extratropics is intermediate to the DARDAR and 2C-ICE values; however, the IWP over the convective land areas in South America and Africa is below both observations. The global average IWP, the tropical average IWP (20°S–20°N), and the ratio between the tropical global averages have been calculated for each data set, and the results are shown in Table 2. The global average IWP from 2C-ICE is largest at 124.9 g m^{-2}, is 46% larger than that from DARDAR, and both are larger than all of the simulations. The CAM4 simulation has the lowest IWP at 37 g m^{-2}, with CAM5 being 50% larger than CAM4 and CAM5/CARMA being 28% larger than CAM5. The CAM5/CARMA IWP at 70.9 g m^{-2} is 17% lower than the DARDAR observation of 85.7 g m^{-2}.

[29] Figure 4 shows scatterplots of the annual average IWP for DARDAR, 2C-ICE, and free-running CAM4, CAM5, and CAM5/CARMA. In these plots the red dots represent tropical values and black dots represent all other latitudes. 2C-ICE consistently has larger values than DARDAR with a slope of 1.46 for the best fit line, but the values are highly correlated ($R^2 = 0.84$) and the values in the tropics have the same spread and bias as values from higher latitudes. The models all have significantly lower IWP than either of the observations and poorer correlations with a maximum R^2 of 0.56 for CAM5/CARMA with DARDAR and a low of 0.28 for CAM4 with 2C-ICE. All models also show that the tropics have a worse fit than higher latitudes. CAM5/CARMA has the best fit with a slope of 0.70 for all values and even closer agreement if just the extratropical values are considered.

[30] The uncertainty in the DARDAR and 2C-ICE IWP is difficult to characterize. Using aircraft data from the Small Particles in Cirrus (SPartICus) campaign [*Mace et al.*, 2009], *Deng et al.* [2013] found 2C-ICE and DARDAR IWC to average 112% and 159%, respectively, of the in situ measurements, but here the 2C-ICE IWP values are ~50 % larger than those from DARDAR. The in situ measurements are

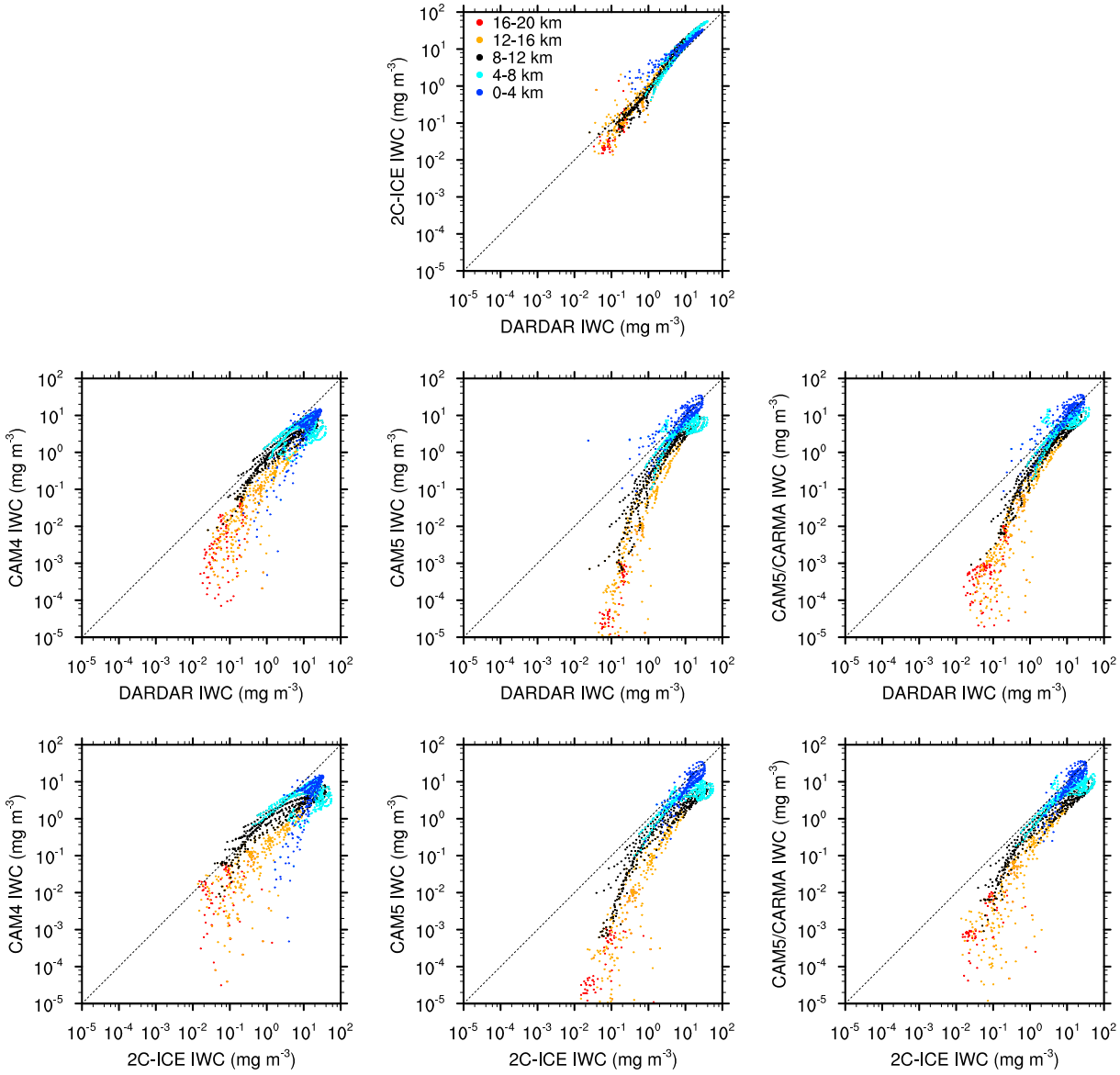

Figure 6. Scatterplots of the annual and zonal average IWC for the same data sets as those in Figure 5. The points are colored based upon the altitude of the data. A one-to-one line is shown on each plot.

based upon optical determination of the particle size distribution and summation of that distribution to get an IWC. The difference in the years used for the climatologies is unlikely to explain such a large difference in the IWP compared to *Deng et al*. [2013], as the year to year variability on the DARDAR data is small. Improved characterization of the magnitude of the retrieval errors would aid model validation. Both observations show a ratio of tropical average to global average IWP of about 1.1, while the simulations are well below this with values of 0.77 for CAM4, 0.75 for CAM5, and 0.85 for CAM5/CARMA, indicating that all of the models are underestimating IWP in the tropics relative to the rest of the planet.

3.1.2. Cloud Fraction and Ice Water Content

[31] Annual and zonal average cloud fraction, in-cloud ice water content (IIWC), and grid-box average ice water content (GIWC) are shown in Figure 5 for DARDAR, 2C-ICE, and the free-running CAM4, CAM5, and CAM5/CARMA simulations. For DARDAR and 2C-ICE, the cloud fraction is the fraction of the observations within a particular grid box that contain a nonzero IWC. For the models, cloud fraction is an arbitrary value diagnosed from the model state by the cloud macrophysics. The DARDAR and 2C-ICE cloud fractions are very similar; however, 2C-ICE excludes clouds that are present in the lower stratosphere of the Southern Hemisphere (SH) polar region. CAM4 and CAM5/CARMA also show clouds at high altitude in the SH polar region, but they are not present in the CAM5 simulation. The CAM5 cloud fraction is significantly larger than either of the observations or the other simulations, which are all in rough agreement.

[32] For IWC, DARDAR and 2C-ICE have similar patterns, again with differences in the SH polar stratosphere. DARDAR shows a little more ice at higher altitudes than 2C-ICE, and 2C-ICE has more grid-box average IWC at lower altitudes. DARDAR shows larger IIWC near the

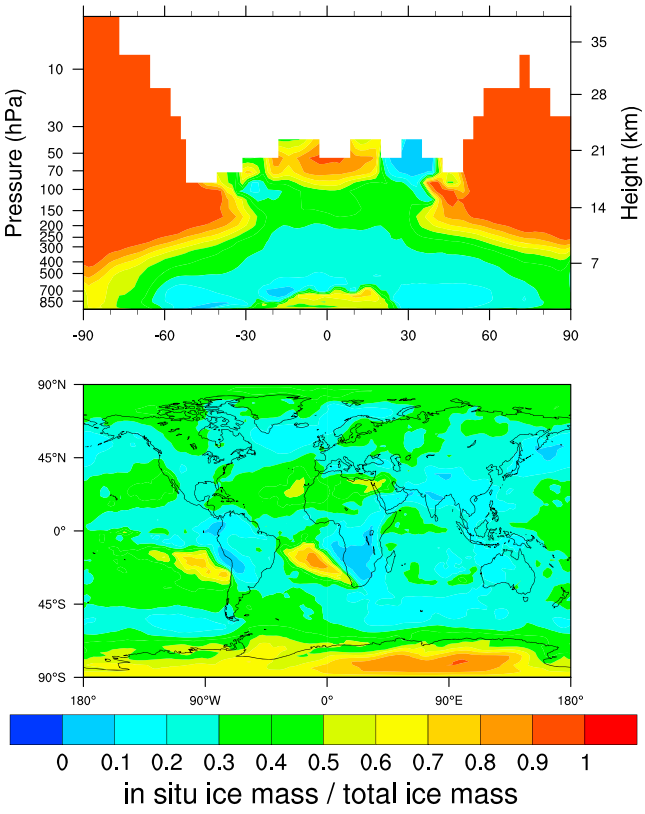

Figure 7. (top) Annual and zonal average ratio of in situ to total ice water content and (bottom) annual average ratio of in situ to total ice water path from the free-running CAM5/CARMA simulation.

surface from 60 to 80°S and 50 to 70°N. All of the simulations have less IWC in the tropics at all altitudes than the observations, although the CAM5/CARMA simulation has the most and the CAM4 has the least. The CAM4 simulation has more IWC at higher altitudes than either the CAM5 or CAM5/CARMA simulations.

[33] Figure 6 shows a scatterplot of the annual and zonal average IWC from DARDAR, 2C-ICE, and the free-running CAM4, CAM5, and CAM5/CARMA models. The data points in these plots are colored by the altitude. DARDAR and 2C-ICE are both less sensitive than the models, with minimum IWC values 10^{-2} mg m^{-3}, while the models have values to 10^{-5} mg m^{-3}. 2C-ICE has larger values for high IWC and smaller values for low IWC than DARDAR. The larger values, which dominate the IWP, explain how 2C-ICE could have a significantly larger IWP than DARDAR. The smaller values, which are more typical of what was measured during SPartICus, explain how DARDAR could overestimate the in situ observations. The models all tend to have a steeper dropoff with lower IWC at higher altitudes than either of the observations.

3.1.3. In Situ Versus Detrained Ice

[34] CAM5/CARMA has two sets of ice bins, those for ice initially detrained by convection and those for ice that was nucleated in situ by the stratiform microphysics. Once categorized, the ice can grow or shrink but remains in that category until it has totally melted or sublimated. Figure 7 shows an annual average of the in situ ice fraction for both a zonal average IWC and a map of IWP. As can be seen, detrained ice is more common, particularly at lower altitudes and over convective landmasses like Southern Africa and South America. Globally averaged, detrained ice accounts for 75% of the total ice mass in the atmosphere. In situ ice is more common near or above the tropopause, over parts of the ocean, and over North Africa and the Antarctic. These are areas that as Figure 3 shows tend to have a very small IWP. *Massie et al.* [2002] estimate that 50% of tropical cirrus over the maritime continent at 100 hPa are formed by convective blow-off and the other half are from in situ formation. For this same region, *Riihimaki and McFarlane* [2010] find 39–44% convective cloud fraction using CALIPSO data and CAM5/CARMA has 60% convective cloud. It would be helpful to have additional observational estimates of this ratio, to determine if models are making ice particles for the right reasons.

3.1.4. Probability Distributions of Effective Radius, IWP, and IWC

[35] Figure 8 shows probability distributions for effective radius, IWP, and IWC calculated using instantaneous output sampled globally for 1 year from DARDAR, 2C-ICE, and the free-running CAM4, CAM5, and CAM5/CARMA models. DARDAR and 2C-ICE have very similar probability density functions of effective radius that look most like the CAM4 model, but all of the models have larger particles than are indicated by DARAR or 2C-ICE. DARDAR, 2C-ICE, and CAM4 rely upon mass-diameter relationships to infer

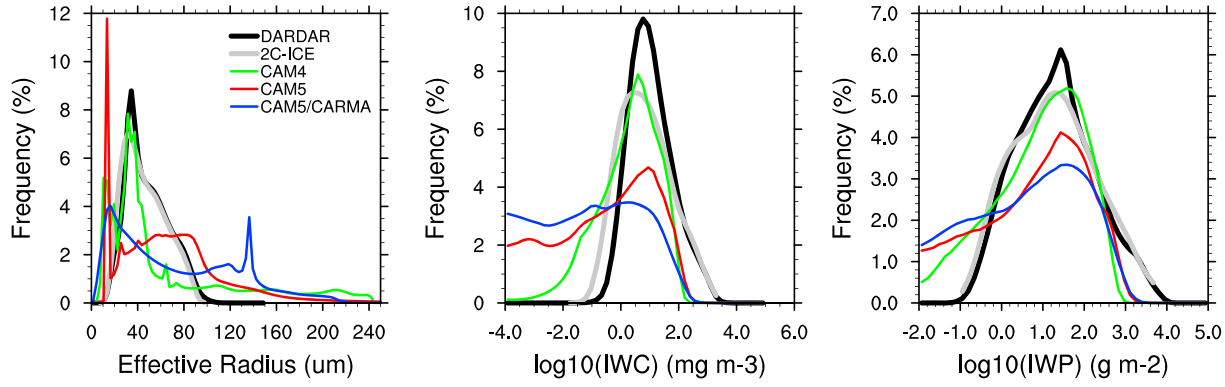

Figure 8. Probability distributions of the instantaneous values of (left) effective radius, (center) IWC, and (right) IWP for the same data sets as those in Figure 1.

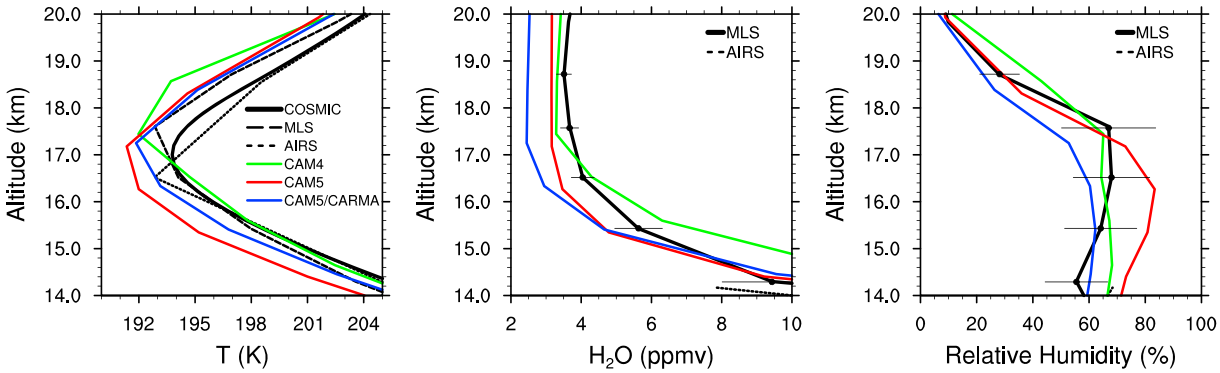

Figure 9. Annual tropical average (left) temperature, (middle) water vapor, and (right) relative humidity from the CAM4, CAM5, and CAM5/CARMA free-running simulations and the COSMIC, MLS, and AIRS observations. Error bars for MLS water vapor and relative humidity are from accuracy estimates in *Livesey et al*. [2011].

particle size. The CAM5 models prognose particle size and show both a peak of smaller particles and more large particles than either the DARDAR or 2C-ICE distributions. For CAM5/CARMA, the peak around 15 μm is from in situ ice and the peak at 140 μm is from detrained ice. For both IWC and IWP, the models have broader distributions with more of the smaller ice values. The models are missing some of the larger IWC and IWP events that are seen in the observations; however, the peaks in all of the distributions occur at similar values. 2C-ICE distributions are slightly clipped at the high end of the IWC and the high and low ends of the IWP distribution. This is likely from some limits applied during the 2C-ICE retrieval process.

3.2. Tropical Analysis

[36] The tropical UTLS is an important region for the transport of water vapor and other tracers into the stratosphere. Here we examine the performance of the models in the UTLS compared to several observations of temperature, water vapor, and relative humidity. For our purposes, the tropics will be defined as the region from latitudes 20°S to 20°N. The results presented are the annual average of the last 5 years of the simulations or multiyear climatologies of the observations.

3.2.1. Temperature, Specific Humidity, and Relative Humidity

[37] Climatologies of several observational products have been used to evaluate the model temperature, water vapor, and relative humidity. The Constellation Observing System for Meteorology, Ionosphere, and Climate (COSMIC) [*Fong et al*., 2008] instruments provide high vertical resolution temperature data from 2006 to 2009. Temperature, water vapor, and relative humidity data are used from the Microwave Limb Sounder (MLS) [*Walters et al*., 2006] on Aura version 3.3 from 2004 to 2012 and from the Atmospheric Infrared Sounder (AIRS) [*Aumann et al*., 2003] version 5.0 from 2002 to 2012. Using Level 2 data, we gridded MLS and COSMIC data on a 1.9° × 2.5° horizontal grid retaining the native vertical resolution. The AIRS data are from their AIRX3STM Level 3 product and are on a 1° × 1° horizontal grid.

[38] Figure 9 shows the annual and tropical average of the vertical profile of temperature from COSMIC and MLS, the water vapor mixing ratio from MLS, and the relative humidity from MLS and AIRS along with the corresponding fields from the CAM4, CAM5, and CAM5/CARMA free-running simulations. All models are colder and have a higher cold-point tropopause than the observations, with CAM5 being the coldest. The temperature plot also shows that there is a bias between COSMIC and MLS temperatures that changes with altitude and is likely to be a problem with the MLS forward model and is a subject of continued research by the MLS team [*Schwartz et al*., 2008]. The CAM4 stratospheric entry value for water vapor is similar to the MLS observation with CAM5 being 0.5 ppm drier than MLS and CAM5/CARMA 1.0 ppm drier than MLS. CAM4 relative humidity is also the best match for the MLS and AIRS observations. CAM5/CARMA is ~10% less humid than CAM4 at most altitudes, while CAM5 is similar to CAM4 in the lower troposphere but is up to 20% more humid in the upper troposphere (14 to 18 km). The MLS observation of relative humidity is likely biased high in the upper troposphere, because of the previously mentioned cold temperature bias in this region in MLS. We stop using the AIRS observation at ~14 km, where the water vapor mixing ratios drop below 10 ppmv. The excess relative humidity in the CAM5 model allows it to have a reasonable stratospheric entry value for water vapor despite its ~3 K cold bias in the cold-point temperature. As expected, CAM5/CARMA has a dry bias in the stratospheric entry value for water vapor because of the ~2.5 K cold bias in the cold-point temperature.

3.2.2. Cloud Condensate, Melting Layer

[39] The annual and tropical average vertical profile of grid-box average cloud condensate and precipitation for CAM4, CAM5, and CAM5/CARMA are shown in Figure 10 along with the corresponding ice water content from DARDAR. CAM4 has a large amount of liquid cloud where the retrievals would suggest it should be ice cloud; however, the total condensate is close to the DARDAR values. Both CAM5 and CAM5/CARMA have significantly less total condensate than is observed by DARDAR; however, the peak in total condensate at ~5.5 km in the models is consistent with the vertical location of the upper peak in the DARDAR data. CAM5/CARMA has significantly more total condensate than CAM5 in the 3 to 9 km range. CAM5 has much of its cold condensate in the form of snow. Snow is diagnostic in CAM5, so this

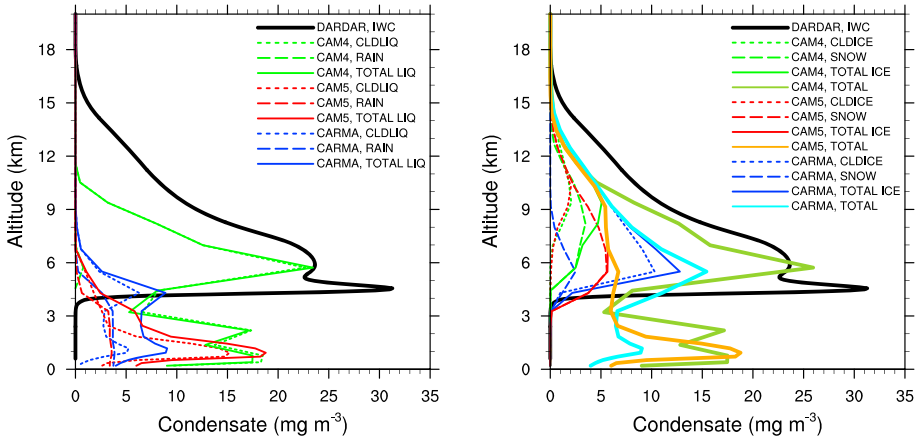

Figure 10. Annual and tropical average of the grid-box average (left) liquid condensate and (right) ice condensate for CAM4, CAM5, and CAM5/CARMA including precipitation compared with the IWC from DARDAR.

means that it is removed from the model at the end of the model's 30 minute time step. CAM5/CARMA does not have autoconversion of ice to snow, so the "snow" is retained as larger ice particles. The only diagnostic snow in CAM5/CARMA comes from the freezing of raindrops.

[40] DARDAR also has a secondary peak at ~4 km that is likely to be from contamination of the retrieval by water drops and/or water-coated ice crystals that generate a higher radar reflectivity [*Sassen et al.*, 2007] and are being misclassified as high amounts of ice condensate. This DARDAR peak corresponds to the melting layer, a peak in the liquid condensate at ~4 km in CAM5/CARMA that is not present in CAM5. CAM4 has a large liquid layer at ~6 km. CAM5/CARMA also has less liquid cloud near 1 km than CAM5. This is because of different tuning of the RHMINL parameter, the minimum relative humidity for the formation of low clouds. Because of the extra ice and liquid cloud present in CAM5/CARMA, it needs fewer low liquid clouds and thus a higher RHMINL for top of atmosphere radiative balance.

3.2.3. Ice Cloud Properties

[41] Figure 11 shows the annual average of the tropical cloud fraction, grid-box average IWC, and in-cloud IWC from the DARDAR and 2C-ICE observations and from the CAM4, CAM5, and CAM5/CARMA free-running models. The CAM5/CARMA ice cloud fraction is in good agreement with both the DARDAR and 2C-ICE values. CAM5 ice cloud fraction peaks a little lower and has a maximum value that is about 50% larger than the observations. Also visible for CAM5/CARMA is the enhancement in liquid cloud fraction at ~4 km from the melting layer and the reduction in low cloud at ~1 km from the tuning of the CAM5/CARMA liquid macrophysics compared to CAM4 and CAM5.

[42] The annual and tropical average in-cloud IWC is shown in Figure 11 (right). Solid curves show the data as reported, while the dashed curves show data that use a −10°C ramp for partitioning into ice and liquid, and the dotted curves show data that use a −20°C ramp. DARDAR data show a large spike at ~4 km, which is likely an artifact of the

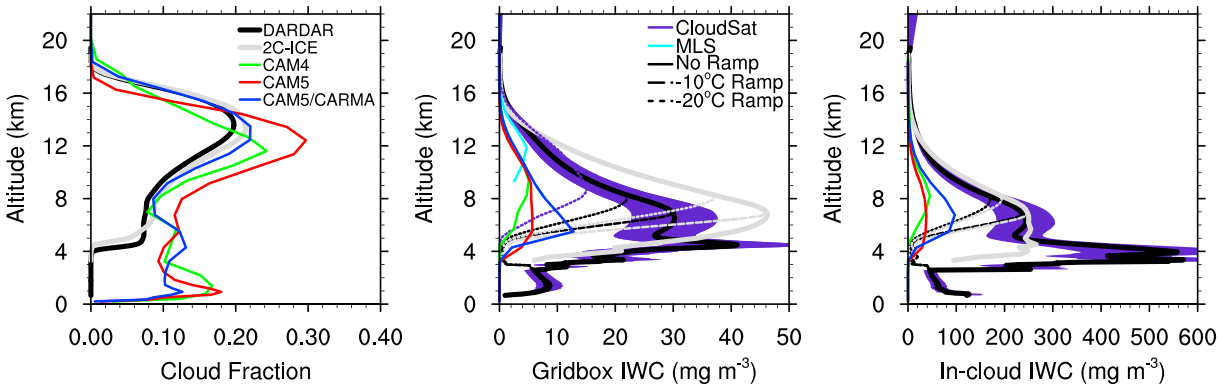

Figure 11. Annual and tropical (left) average cloud fraction, (middle) grid-box average ice water content, and (right) in-cloud ice water content from DARDAR, 2C-ICE, MLS, CloudSat, and simulations using the free-running CAM4, CAM5, and CAM5/CARMA. The dotted curves are based upon a −20°C ramp and the dashed curves a −10°C ramp for partitioning the condensate into ice and liquid. All simulations are reporting a combination of cloud ice and snow for the IWC. The shaded area is the IWC error reported by DARDAR for the no-ramp case.

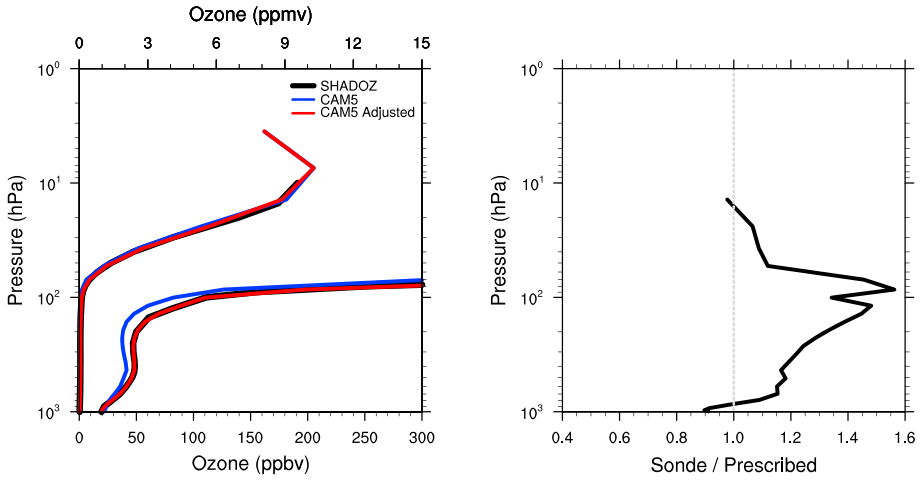

Figure 12. (left) Annual average ozone vertical profiles using two scales, ppmv for the stratosphere and ppbv for the troposphere, from SHADOZ tropical stations (black) compared with tropically averaged prescribed ozone used by CAM5 (blue) and adjusted to match SHADOZ (red). (right) Annual average vertical profile of the scaling factor used to correct the CAM5 prescribed ozone.

melting layer. Using the −10°C ramp eliminates this source of contamination. For the models, the IWC is the sum of the cloud ice and the snow diagnosed by the model. The DARDAR and 2C-ICE in-cloud values are in good agreement with each other above the melting layer and are both ~2–3 times the magnitude of the CAM5/CARMA values, which is ~2 times the CAM4 and CAM5 values. The peak in the CAM5/CARMA IWC does occur at a similar altitude to DARDAR and 2C-ICE. CAM4 peaks at a higher altitude. The small difference in DARDAR and 2C-ICE cloud fraction leads to a larger difference in grid-box average IWC, with the 2C-ICE values 50% larger than DARDAR. Both are also larger than values from MLS or CloudSat IWC, and all of the observations are larger than the values from any of the models. The larger CAM5 cloud fraction does reduce some of the difference with CAM5/CARMA in the grid-box average IWC that was seen in the in-cloud IWC; however, CAM5/CARMA still has the largest IWC of any of the simulations.

3.2.4. Sensitivity to Prescribed Ozone

[43] The free-running models all have cold-point and stratospheric temperatures that are colder than observations. Ozone is a source of heating in the stratosphere, and the ozone in CAM is prescribed from a monthly climatology. One possibility for why CAM is too cold is that the prescribed ozone file is biased in the tropics. To check this, we compared the monthly average prescribed ozone values with a monthly average of the tropical sondes from the Southern Hemisphere Additional Ozonesondes (SHADOZ) network [*Thompson et al.*, 2007; *Tilmes et al.*, 2012] using data from 1998 to 2011. Figure 12 shows the annual average values for the tropical SHADOZ data and the CAM prescribed ozone file. The SHADOZ data are well matched by the CAM prescribed ozone field in the stratosphere, but the CAM ozone has a negative bias near the tropopause where there is a sharp ozone gradient. The annual average difference can be as much as 60% at ~100 hPa and is as much as 80% for some months.

[44] Figure 13 shows the results of free-running CAM5 and CAM5/CARMA simulations that use a prescribed ozone file that has been scaled each month to correct for the monthly average ozone bias relative to the SHADOZ sondes. The cold-point temperature for CAM5 is still ~1 K too cold but for CAM5/CARMA is now in good agreement with the COSMIC annual average; however, a cold bias of ~3.5 K for CAM5 and ~1.5 K for CAM5/CARMA still

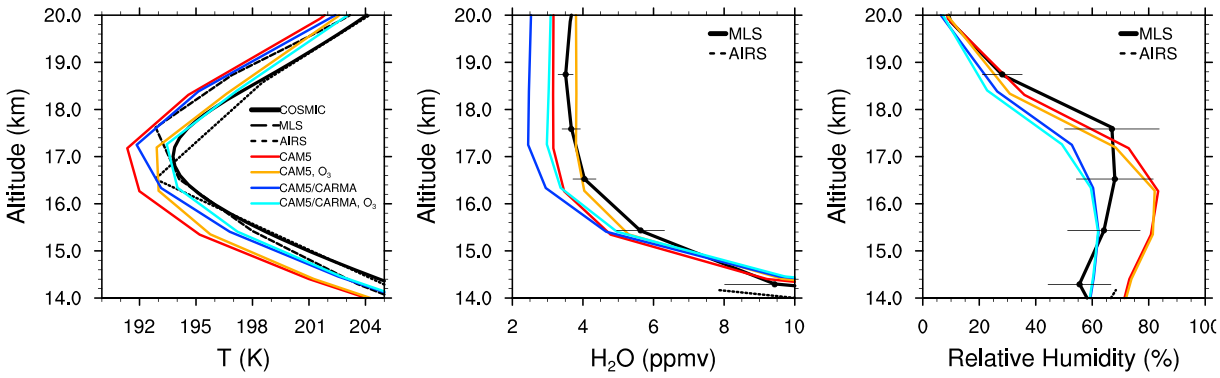

Figure 13. Similar to Figure 6 but including results from the CAM5 O_3 and CAM5/CARMA O_3 runs using the free-running models with the prescribed ozone scaled to match SHADOZ.

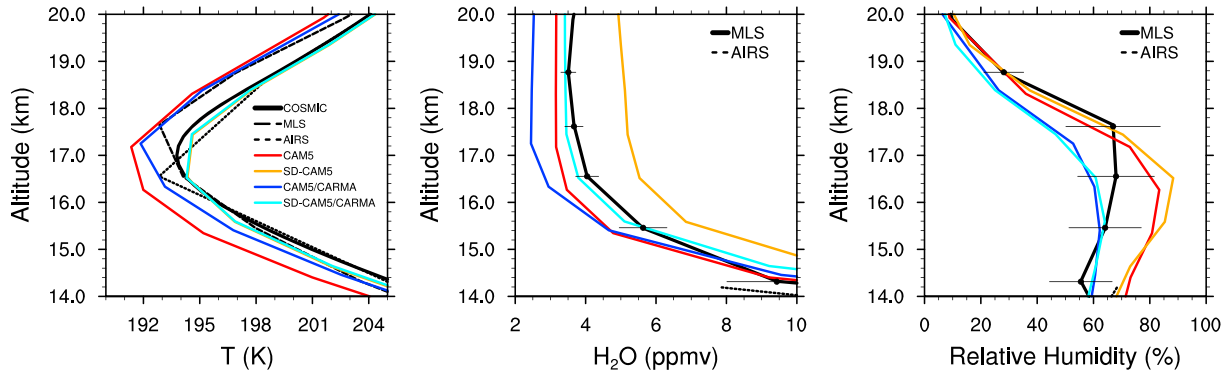

Figure 14. Similar to Figures 6 and 10 but includes SD-CAM5 and SD-CAM5/CARMA runs where the temperature and dynamics are nudged to the GEOS5-DAS assimilation data.

exists in the upper troposphere and a ~1 K bias exists in the stratosphere. The relative humidity is largely unchanged resulting in a stratospheric entry value for water vapor CAM5 that is in good agreement with the MLS data. For CAM5/CARMA, the water vapor stratospheric entry value is 0.5 ppm drier than the MLS data but is similar to the value from CAM5 using the uncorrected ozone file and 0.5 ppm wetter than CAM5/CARMA with the uncorrected ozone file.

3.2.5. Sensitivity to Specified Dynamics

[45] The CAM5 models can be run nudged to an observed meteorology. Figure 14 shows the results of CAM5 and CAM5/CARMA simulations using the GEOS5-DAS 5.2 meteorology files for the period 2007–2010. The nudged temperature is in good agreement with the COSMIC data although perhaps slightly warmer at the cold point and 0.5 K colder in the upper troposphere. The relative humidity for CAM5/CARMA is largely unchanged from the free-running model; however, the CAM5 relative humidity is 5–10% larger than the free-running model. For CAM5/CARMA, the relative humidity results in an average water vapor mixing ratio that is in excellent agreement with the MLS annual average value; however, for CAM5 this results in a water vapor mixing ratio at the cold point that is ~1.5 ppmv larger than MLS.

[46] Figure 15 shows the time series of the tropical water vapor anomaly, also known as the water vapor tape recorder [*Mote et al.*, 1996] for the period 2007 to 2013 from MLS and for the same period from the SD-CAM5 and SD-CAM5/CARMA runs. There is good agreement in both the magnitude and timing of the anomaly between MLS and CAM5/CARMA, but it appears that the model may still be spinning up during the first 2 years of the time series. The CAM5 tape recorder shows an increasing trend

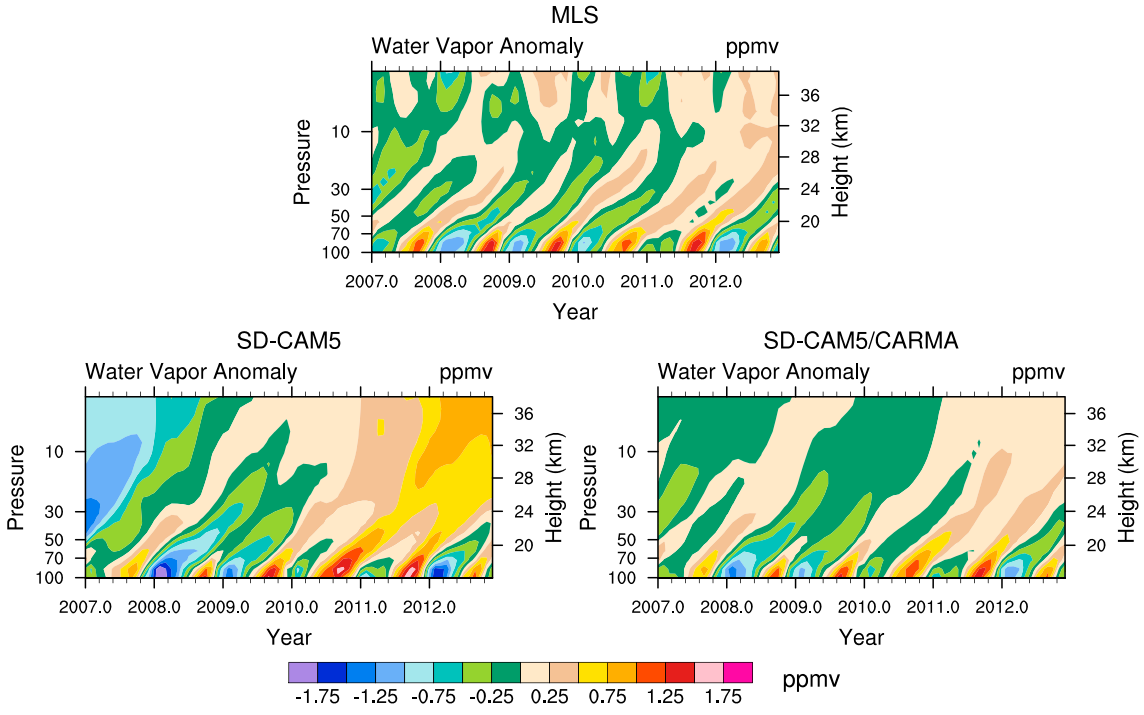

Figure 15. The tropical water vapor anomaly time series from MLS, CAM5, and CAM5/CARMA with specified meteorology from GEOS5-DAS for the period 2007–2013.

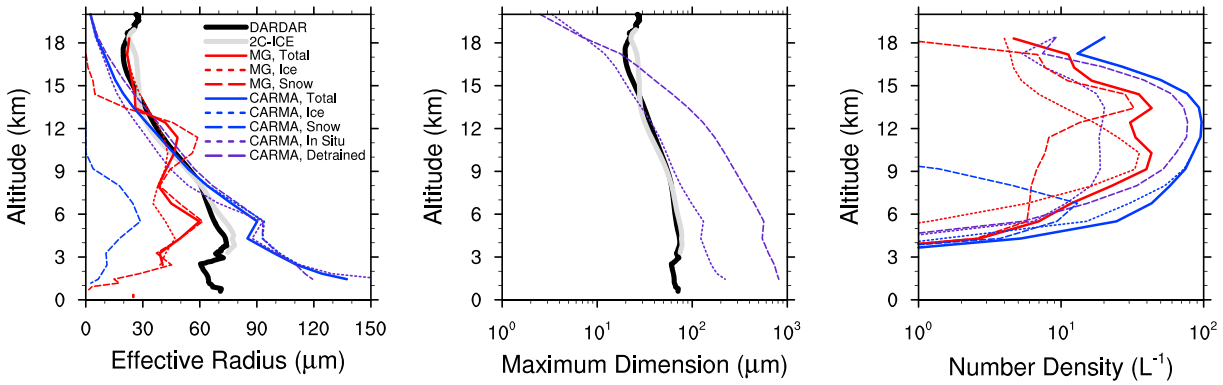

Figure 16. Annual and tropical average vertical profiles of ice particle effective radius, maximum dimension, and number density for DARDAR, 2C-ICE, and free-running simulations from CAM5 (MG) and CAM5/CARMA. (left) Average in-cloud effective radius using *Mitchell* [2002] and (middle) average maximum dimension. In DARDAR and CAM5, particles are assumed to be spheres, so the maximum dimension is the same as the spherical radius. (right) In-cloud ice particle number density for CAM5 and CAM5/CARMA.

during the entire time period, and the anomalies near the tropopause tend to be larger than those seen in either MLS or CAM5/CARMA. The trend and larger anomalies are likely caused by the high relative humidities in the CAM5 model. The MLS anomaly shows structure above 32 km that is not present in either simulation. This is because CAM5 does not include stratospheric chemistry and is missing the production of water from methane oxidation. Taken together, Figures 14 and 15 show that CAM5/CARMA is able to reproduce the observed mean and variability of the UTLS water vapor in the tropics when supplied with the correct temperature and winds.

3.2.6. Effective Radius, Maximum Dimension, and Number Density

[47] Figure 16 shows the annual and tropical average effective radius, maximum dimension, and number density. Effective radius is calculated using *Mitchell* [2002],

$$r_{\text{eff}} = \frac{3}{4}\frac{\text{IWC}}{\rho_i P_t} \tag{17}$$

where IWC is the ice water content, ρ_i is the ice density, and P_t is the total projected area. This effective radius is used by the CAM5 radiation code for determining cloud optical properties. Retrievals of ice effective radius are difficult, and DARDAR and 2C-ICE rely upon finding a best fit for the observed radiances based upon the forward model's assumptions of the particle size distribution. Figure 16 (left) shows that the CAM5 ice effective radius is a good match for the DARDAR and 2C-ICE effective radius above 11 km but does have some oscillations that are not seen in the data and is smaller than the data at lower altitudes. CAM5/CARMA has smaller particles than either CAM5 or the observations above 11 km but is smoother than CAM5 like the observations and is a better match but trending larger than the observations below 11 km. In CAM5/CARMA, there is a decrease in effective radius near the melting layer at ~4 km and the in situ ice particles have a smaller effective radius and a smaller average maximum diameter than the detrained ice particles throughout the entire altitude range. The average maximum diameter for both in situ and detrained ice increases with decreasing altitude to almost 1 mm but shows a decrease at the melting layer.

[48] Figure 16 (right) shows the annual and tropical average in-cloud number density for the free-running CAM5 and CAM5/CARMA simulations. Both models show a peak in total number density at 13.5 km, with CAM5/CARMA having about ~50% more particles at the peak than CAM5. At the peak of the number density, CAM5 has mostly snow particles, while the peak in ice particle number density is around 10 km. This is in contrast to the mass which in Figure 13 was shown to peak at ~11 km for CAM5 cloud ice and 6 km for snow. CAM5/CARMA has mostly detrained ice at the altitude of the peak number density; however, the in situ ice also peaks at about the same altitude but makes up less than 15% of the total number. This contrasts with a mass peak for cloud ice in CAM5/CARMA at ~6 km. There are only small amounts of snow in CAM5/CARMA, and number density peaks at 6.5 km consistent with the altitude of its snow mass peak.

Table 3. Global and 1085 Annual Averaged Energy Diagnostic Fields in W m^{-2} for the 1086 CAM5 and CAM5/CARMA Free-Running Models and Observations From CERES 1087 and ISCCP[a]

Field	CAM5	CAM5/CARMA	CERES	ISCCP
RESTOM	−1.0	−1.0		
RESSURF	−1.0	−1.0		
RESTOA	1.2	1.2	0.8	
FLDS	**343.1**	340.3		343.3
FLUT	237.7	**240.5**	239.6	
FLUTC	258.7	**261.3**	269.4	
FLNT	236.3	239.1		
FSDS	183.9	**187.7**		189.3
FSNTOA	**238.9**	241.7	240.4	
FSNTOAC	289.2	**288.9**	287.5	
FSNT	235.3	238.1		
LWCF	**21.0**	20.8	29.9	
SWCF	−50.3	**−47.2**	−47.1	

[a]The model field in bold is closest to the observation.

3.3. Global Energy Balance

[49] As we have shown, CAM5 and CAM5/CARMA have different distributions of cloud condensate, cloud fraction, water vapor, and temperature. These changes can affect the energy balance within the model. Table 3 shows global and annual average values for key energy diagnostics from the CAM5 and CAM5/CARMA free-running models and the corresponding observations from Clouds and Earth's Radiant Energy Systems (CERES) Energy Balanced and Filled [*Wielicki et al*., 1996] version 2.4 or International Satellite Cloud Climatology Project (ISCCP) [*Schiffer and Rossow*, 1983]. The low cloud in CAM5/CARMA is tuned via RHMINL to give a residual energy imbalance at the top of model (RESTOM), top of atmosphere (RESTOA), and surface (RESSURF) of the model that are very similar to CAM5 values. RHMINL also has a significant impact on the shortwave cloud forcing (SWCF), with CAM5 having a $-3\,\mathrm{W\,m^{-2}}$ bias compared to CERES2 that is absent in the CAM5/CARMA simulation. The shortwave downwelling flux at the surface is also improved by $3.8\,\mathrm{W\,m^{-2}}$ in CAM5/CARMA, although it is still $1.6\,\mathrm{W\,m^{-2}}$ from the ISCCP value.

[50] The longwave cloud forcing (LWCF) is very similar between the two models and $9\,\mathrm{W\,m^{-2}}$ below the CERES value. There is a $3.2\,\mathrm{W\,m^{-2}}$ difference in the downward longwave flux at the surface (FLDS) between CAM5 and CAM5/CARMA, with CAM5 agreeing better with CERES. However, CAM5 has a longstanding bias in the total (FLUT) and clear-sky (FLUTC) longwave upwelling flux at the top of the model that is improved by $1.0\,\mathrm{W\,m^{-2}}$ and $2.6\,\mathrm{W\,m^{-2}}$, respectively, in CAM5/CARMA.

4. Summary and Discussion

[51] We have constructed CAM5/CARMA, a GCM with sectional microphysics for cirrus clouds that improves upon both the bulk cloud scheme used in CAM4 and the two-moment cloud scheme being used in CAM5. Cloud metrics like cloud fraction, ice water content, and ice water path are all improved in CAM5/CARMA and compare better with the DARDAR and 2C-ICE retrieval products; however, all of the models still underestimate the IWC and IWP particularly in the convective areas of the tropics compared to DARDAR and 2C-ICE. CAM5/CARMA also does better in the mixed-phase region, generating a melting layer that is absent in the CAM5 model. One of the main reasons for the improved simulations of ice and of the melting layer is the use of prognostic snow in CAM5/CARMA. CAM5 diagnoses snow, which means that it autoconverts the large ice to snow and then removes the snow from the model at the end of the time step, faster than the snow would have been able to sediment to the ground. This results in lower ice mass and reduces the amount of ice that is able to sediment through the area of melting temperatures, generating a weaker melting layer. The use of the *Wilson and Ballard* [1999] subgrid-scale saturation scheme in CAM5/CARMA increases the amount of ice mass relative to the other models and results in relative humidity that is in better agreement with observations.

[52] The standard CAM models use a prescribed ozone file to provide heating in the stratosphere and upper troposphere. Comparison of this file to averages from SHADOZ sondes in the tropics indicates that a major reason for the cold bias in the tropical cold-point tropopause for the free-running CAM5/CARMA model is a negative bias in the ozone profile near the sharp ozone gradient around the tropopause. For CAM5/CARMA, correcting these errors results in good agreement between the model and the COSMIC temperatures at the cold point and an improvement with the MLS water vapor. For CAM5, there is still an ~1 K cold bias in the cold-point temperature but good agreement with the MLS water vapor. The prescribed ozone file was generated using a CAM-CHEM run with interactive chemistry. It would be interesting to know why this model produced a biased ozone field. Perhaps running CAM-CHEM at a higher vertical resolution and with specified dynamics would help capture the sharp ozone gradient.

[53] CAM5/CARMA has improved temperature and water vapor in the tropics compared to the other CAM models and, when run with either specified dynamics or with a prescribed ozone file corrected to match SHADOZ observations, yields a tropical cold-point temperature, water vapor mixing ratio, and relative humidity that are in good agreement with COSMIC, MLS, and AIRS observations. There is a lot of uncertainty in observations of upper tropospheric relative humidity, but CAM5 relative humidity is probably unrealistic and results in high entry values for water vapor when temperatures are corrected to match observations.

[54] CAM5/CARMA tracks both in situ and detrained ice, and we find that detrained ice is generally much more important in the model, with in situ ice only important near or above the tropopause. Globally, 75% of the ice mass is from detrained ice particles and 25% is from in situ nucleation. It is hard to know what the proper ratio should be for these types of particles. The diffusivity measurements shown in Figure 2 suggest that convection in the tropics could go a little higher on occasion than occurs in the models; however, this might reduce the role of in situ ice formation even more. We used temperature-dependent size distributions from observed clouds to connect the detrainment process to the large scale, but perhaps this overestimates the amount of detrained ice and maybe some of the condensate should instead enter as water vapor giving more opportunities for in situ ice formation. It might also be that detrainment spreads to the grid-box average too quickly and that a subcolumn approach is needed to provide regions in the grid box for in situ ice to form away from detrained ice which would otherwise take up any water in excess of ice saturation. The coarse vertical grid resolution and the large diffusivities may also cause the detrained ice to move higher than its detrainment level. Perhaps in a coarse grid model the vertical diffusivity should be lowered since there is already some numerical diffusion. However, it might also be that ice particles formed in convection are more numerous, carry more of the mass, and are radiatively more important than ice formed in situ on the large scale. In the CAM5/CARMA simulations, we neglected heterogeneous nucleation, which *Gettelman et al*. [2012] showed was of secondary importance. Despite this, we still had improved cirrus simulations over those in CAM5 that does include heterogeneous nucleation. Recent observations from *Cziczo et al*. [2013] suggest a much more important role for heterogeneous nucleation with dust ice nuclei than has typically been assumed. This could affect the ratio of in situ to detrained ice and the amount of cirrus and warrants future study.

[55] Introduction of a new cloud scheme required retuning of the model. For CAM5/CARMA, we chose a different cloud

fraction scheme than is used in CAM5, and we tuned the model to have lower average ice cloud fraction like the average vertical profiles of DARDAR and 2C-ICE observations. Despite having lower ice cloud fractions than CAM5, the CAM5/CARMA model with increased middle and upper tropospheric condensate still needs a reduction in low-level liquid cloud to stay in agreement with top of atmosphere energy balance. This reduction is accomplished by increasing the critical relative humidity threshold for low cloud formation and improving the shortwave cloud forcing by $3\,W\,m^{-2}$ and the downward shortwave radiation at the surface by $3.8\,W\,m^{-2}$ in CAM5/CARMA. The longwave cloud forcing is largely unchanged, but there are small improvements in upward longwave flux at the top of the atmosphere for all sky and clear sky of 1.0 and $2.6\,W\,m^{-2}$, respectively. All CAM models have less cloud ice than the DARDAR and 2C-ICE observations, suggesting that the CAM4 and CAM5 models may be compensating by adding additional low cloud for shortwave energy balance.

[56] Since CAM5/CARMA neglects heterogeneous ice nucleation, this might lead to too much condensate in the regions near the freezing level that should be removed by ice. Modeling studies by *Lohmann* [2002] and *Demott et al*. [2010] have shown an ice glaciation aerosol feedback in which increased ice nucleation from heterogeneous nucleation at low supersaturations increases precipitation and lowers the liquid water path, mostly in mid to high latitudes. In the tropics, the increases in ice and liquid cloud by including prognostic precipitation and subgrid scale saturation in CAM5/CARMA are likely to be more significant than the ice glaciation feedback. Diagnostic snow in CAM5 removes snow size particles at the end of the time step even if their fall velocities were not sufficient for them to fall to the ground. CAM5/CARMA with prognostic snow does not do this, and thus all snow must sediment to the ground before being removed. This results in a larger amount of elevated ice and liquid condensate and a pronounced melting layer absent in CAM5. The melting layer is seen in observations, and heterogeneous ice nucleation seems unlikely to significantly reduce its magnitude, so we think in the tropics some adjustment in low clouds will be necessary. Heterogeneous nucleation may be more important in other regions, and further study including heterogeneous ice nucleation is warranted.

[57] CAM5/CARMA ice particles have a smaller effective radius in the tropical upper troposphere than the ice particles in either CAM5 or the DARDAR or 2C-ICE retrievals. If true, this could explain some of the differences in the IWC estimates as smaller particles have a stronger mass extinction in the shortwave. Are the parameterizations used to predict particle size in the forward models of the retrievals allowing for sufficiently small particles?

[58] Since it is a sectional model with 74 additional advected tracers, the CAM5/CARMA cirrus model takes ~4 times longer to run than CAM5 and is not intended for hundreds of year integrations; however, it can easily be run for tens of years and many of the lessons learned here can be used to improve the less expensive cloud parameterizations and improve our knowledge of the processes involved.

[59] Many of the changes that improved the quality of the CAM5/CARMA simulations can be applied to CAM5 with the standard Morrison-Gettelman microphysics including the following:

[60] 1. lowering the eddy diffusivity in the free troposphere,

[61] 2. improving the prescribed ozone file compared to SHADOZ,

[62] 3. using a prognostic treatment of snow,

[63] 4. removing ice/snow autoconversion and the separate snow hydrometeor,

[64] 5. lowering the ice cloud fraction,

[65] 6. using subgrid-scale water vapor for nucleation and growth of ice clouds, and

[66] 7. using subgrid-scale water vapor for nucleation and growth of liquid clouds.

[67] Work is already underway to include prognostic snow in the next version of the Morrison-Gettelman microphysics, and some of the other changes are being considered.

[68] **Acknowledgments.** Portions of this research were supported by an NCAR ASP Fellowship and NASA Grants NNX10AO53A (ATTREX) and NNX09AK71G (MAP). Julien Delanoë's research is partly funded by CNES (Centre National d'Études Spatiales). Thank you to the COSMIC, MLS, AIRS, CloudSat, and CALIPSO teams for making their data products available and for assistance in the use of those products. Thanks also to Jeffrey Taylor for making his gridded COSMIC data set available for this work. Computing resources supporting this work were provided by the NASA High-End Computing (HEC) Program through the NASA Advanced Supercomputing (NAS) Division at Ames Research Center and by the Climate Simulation Laboratory at NCAR's Computational and Information Systems Laboratory (CISL), sponsored by the National Science Foundation and other agencies. We wish to thank the ICARE Data and Services Center for providing access to the DARDAR data used in this study. The CESM project is supported by the National Science Foundation and the Office of Science (BER) of the U.S. Department of Energy. NCAR is sponsored by the National Science Foundation.

References

Alappattu, D. P., and P. K. Kunhikrishnan (2010), First observations of turbulence parameters in the troposphere over the Bay of Bengal and the Arabian Sea using radiosonde, *J. Geophys. Res.*, *115*, D06105, doi:10.1029/2009JD012916.

Aumann, H. H., et al. (2003), AIRS/AMSU/HSB on the Aqua mission: Design, science objectives, data products, and processing systems, *IEEE Trans. Geosci. Remote Sens.*, *41*(2), 253–264.

Bardeen, C. G., O. B. Toon, E. J. Jensen, D. R. Marsh, and V. L. Harvey (2008), Numerical simulations of the three-dimensional distribution of meteoric dust in the mesosphere and upper stratosphere, *J. Geophys. Res.*, *113*, D17202, doi:10.1029/2007JD009515.

Chen, W.-T., C. P. Woods, J.-L. F. Li, D. E. Waliser, J.-D. Chern, W.-K. Tao, J. H. Jiang, and A. M. Tompkins (2011), Partitioning CloudSat ice water content for comparison with upper tropospheric ice in global atmospheric models, *J. Geophys. Res.*, *116*, D19206, doi:10.1029/2010JD015179.

Comstock, J. M., T. P. Ackerman, and G. G. Mace (2002), Ground-based lidar and radar remote sensing of tropical cirrus clouds at Nauru Island: Cloud statistics and radiative impacts, *J. Geophys. Res.*, *107*(D23), 4714, doi:10.1029/2002JD002203.

Comstock, J. M., et al. (2006), An intercomparison of microphysical retrieval algorithms for upper-tropospheric ice clouds, *Bull. Am. Meteorol. Soc.*, *88*, 191–204, doi:10.1175/BAMS-88-2-191.

Corti, T., B. P. Luo, Q. Fu, H. Vömel, and T. Peter (2006), The impact of cirrus clouds on tropical troposphere-to-stratosphere transport, *Atmos. Chem. Phys.*, *6*, 2539–2547.

Cziczo, D. J., K. D. Froyd, C. House, E. J. Jensen, M. Diao, M. A. Zondio, J. B. Smith, C. H. Twohy, and D. M. Murphy (2013), Clarifying the dominant sources and mechanisms of cirrus cloud formation, *Science*, *340*, doi:10.1126/science.1234145.

Danielsen, E. F. (1993), In situ evidence of rapid, vertical, irreversible transport of lower tropospheric air into the lower tropical stratosphere by convective cloud turrets and by larger-scale upwelling in tropical cyclones, *J. Geophys. Res.*, *98*(D5), 8665–8681, doi:10.1029/92JD02954.

de Reus, M., et al. (2009), Evidence for ice particles in the tropical stratosphere from in-situ measurements, *Atmos. Chem Phys.*, *9*, 6775–6792.

Delanoë, J., and R. J. Hogan (2008), A variational scheme for retrieving ice cloud properties from combined radar, lidar, and infrared radiometer, *J. Geophys. Res.*, *113*, D07204, doi:10.1029/2007JD009000.

Delanoë, J., and R. J. Hogan (2010), Combined CloudSat-CALIPSO-MODIS retrievals of the properties of ice clouds, *J. Geophys. Res.*, *115*, D00H29, doi:10.1029/2009JD012346.

Delanoë, J., R. J. Hogan, R. M. Forbes, A. Bodas-Salcedo, and T. H. M. Stein (2011), Evaluation of ice cloud representation in the ECMWF and UK Met Office models using CloudSat and CALIPSO data, *Q. J. Roy. Meteorol. Soc.*, *137*, 2064–2078, doi:10.1002/qj.882.

DeMott, P. J., A. J. Prenni, S. M. Kreidenweis, M. D. Petters, C. H. Twohy, M. S. Richardson, T. Eidhammer, and D. C. Rodgers (2010), Predicting global atmospheric ice nuclei distributions and their impacts on climate, *Proc. Natl. Acad. Sci.*, *107*, 11,217–11,222, doi:10.1073/pnas.0910818107.

Deng, M., G. G. Mace, Z. Wang, and H. Okamoto (2010), Tropical Composition, Cloud and Climate Coupling Experiment validation for cirrus cloud profiling retrieval using CloudSat radar and CALIPSO lidar, *J. Geophys. Res.*, *115*, D00J15, doi:10.1029/2009JD013104.

Deng, M., G. G. Mace, Z. Wang, and R. P. Lawson (2013), Evaluation of several A-Train Ice Cloud Retrieval Products with in situ measurements collected during the SPartICus Campaign, *J. Appl. Meteorol. Climatol.*, *52*, 1014–1030, doi:10.1175/JAMC-D-12-054.1.

English, J. M., O. B. Toon, M. J. Mills, and F. Yu (2011), Microphysical simulations of new particle formation in the upper troposphere and lower stratosphere, *Atmos. Chem. Phys.*, *11*, doi:10.5194/acp-11-9303-2011.

Fong, C.-J., et al. (2008), FORMOSAT-3/COSMIC constellation spacecraft system performance: After one year in orbit, *IEEE Trans. Geosci. Remote Sens.*, *46*, 3,380–3,394, doi:10.1109/TGRS.2008.2005203.

Gettelman, A., and T. Birner (2007), Insights into tropical tropopause layer processes using global models, *J. Geophys. Res.*, *112*, D23104, doi:10.1029/2007JD008945.

Gettelman, A., et al. (2010a), Multimodel assessment of the upper troposphere and lower stratosphere: Tropics and global trends, *J. Geophys. Res.*, *115*, D00M08, doi:10.1029/2009JD013638.

Gettelman, A., X. Liu, S. J. Ghan, H. Morrison, S. Park, A. J. Conley, S. A. Klein, J. Boyle, D. L. Mitchell, and J.-L. F. Li (2010b), Global simulations of ice nucleation and ice supersaturation with an improved cloud scheme in the Community Atmosphere Model, *J. Geophys. Res.*, *114*, D18215, doi:10.1029/2009JD013797.

Gettelman, A., X. Liu, D. Barahona, U. Lohmann, and C. Chen (2012), Climate impacts of ice nucleation, *J. Geophys. Res.*, *117*, D20201, doi:10.1029/2012JD017950.

Goff, J. A., and S. Gratch (1946), Low-pressure properties of water from −160 to 212 F, *Trans. Am. Soc. Heat. Air Cond.*, *52*, 95–122.

Heymsfield, A. J. (2007), On measurements of small ice particles in clouds, *Geophys. Res. Lett.*, *34*, L23812, doi:10.1029/2007GL030951.

Heymsfield, A. J., and C. D. Westbrook (2010), Advances in the estimation of ice particle fall speeds using laboratory and field measurements, *J. Atmos. Sci.*, *67*, doi:10.1175/2010JAS3379.1.

Heymsfield, A. J. C., A. B. Schmitt, and C. H. Twohy (2010), Improved representation of ice particle masses based on observations in natural clouds, *J. Atmos. Sci.*, *67*, doi:10.1175/2010JAS3507.1.

Hurrell, J. W., et al. (2013), The Community Earth System Model: A framework for collaborative research, *Bull. Am. Meteorol. Soc.*, *94*, 1339–1360, doi:10.1175/BAMS-D-12-00121.1.

Jacobson, M. Z., R. P. Turco, E. J. Jensen, and O. B. Toon (1994), Modeling coagulation among particles of different composition and size, *Atmos. Environ.*, *28*(7), 1327–1338.

Jensen, E. J., O. B. Toon, L. Pfister, and H. B. Selkirk (1996), Dehydration of the upper troposphere and lower stratosphere by subvisible cirrus clouds near the tropical tropopause, *Geophys. Res. Lett.*, *23*, 825–828.

Jensen, E. J., A. S. Ackerman, and J. A. Smith (2007), Can overshooting convection dehydrate the tropical tropopause layer?, *J. Geophys. Res.*, *112*, D11209, doi:10.1029/2006JD007943.

Jiang, J. H., et al. (2012), Evaluation of cloud and water vapor simulations in CMIP5 climate models using NASA "A-Train" satellite observations, *J. Geophys. Res.*, *117*, D14105, doi:10.1029/2011JD017237.

Koop, T. B., L. A. Tslas, and T. Peter (2000), Water activity as the determinant for homogeneous ice nucleation in aqueous solutions, *Nature*, *406*, 611–614.

Korolev, A. V., G. A. Isaac, S. G. Cober, J. W. Strapp, and J. Hallett (2003), Microphysical characterization of mixed-phase clouds, *Q. J. Roy. Meteorol. Soc.*, *129*, doi:10.1256/qj.01.204.

Korolev, A. V., E. F. Emery, J. W. Strapp, S. G. Cober, G. A. Isaac, M. Wasey, and D. Marcotte (2011), Small ice particles in tropospheric clouds: Fact or artifact? Airborne Icing Instrumentation Evaluation Experiment, *Bull. Am. Meteorol. Soc.*, *92*, doi:10.1175/2010BAMS3141.1.

Kunz, A., L. Pan, P. Konopka, D. Kinnison, and S. Tilmes (2011), Chemical and dynamical discontinuity at the extratropical tropopause based on START08 and WACCM analysis, *J. Geophys. Res.*, *116*, D24302, doi:10.1029/2011JD016686.

Lamarque, J.-F., et al. (2011), CAM-chem: Description and evaluation of interactive atmospheric chemistry in CESM, *Geosci. Model Dev.*, *5*, 369–411, doi:10.5194/gmd-5-369-2012.

Lawson, R. P. (2011), Effects of ice particles shattering on the 2D-S probe, *Atmos. Meas. Tech.*, *4*, 1361–1381, doi:10.5194/amt-4-1361-2011.

Li, J.-L. F., et al. (2012), An observationally based evaluation of cloud ice water in CMIP3 and CMIP5 GCMs and contemporary reanalyses using contemporary satellite data, *J. Geophys. Res.*, *117*, D16105, doi:10.1029/2012JD017640.

Liou, K. N. (1986), Influence of cirrus clouds on weather and climate processes: A global perspective, *Mon. Weather Rev.*, *114*, 1167–1199.

Livesey, N. J., et al. (2011), Earth Observing System (EOS) Aura Microwave Limb Sounder (MLS) Version 3.3 Level 2 data quality and description document, *Jet Propulsion Lab*, JPL D-33509.

Lohmann, U. (2002), A glaciation indirect aerosol effect caused by soot aerosols, *Geophys. Res. Letts.*, *29*(4), 1052, doi:10.1029/2001GL014357.

Mace, J., E. Jensen, G. McFarquhar, J. Comstock, T. Ackerman, D. Mitchell, X. Liu, and T. Garrett (2009), SPartICus: Small particles in cirrus science and operations plan, *Publications (E)*, Paper 33.

Massie, S., A. Gettelman, W. Randel, and D. Baumgardner (2002), Distribution of tropical cirrus in relation to convection, *J. Geophys. Res.*, *107*(D21), 4591, doi:10.1029/2001JD001293.

Mitchell, D. L. (2002), Effective diameter in radiation transfer: General definition, applications and limitations, *J. Atmos. Sci.*, *59*, 2330–2346.

Morrison, H., and A. Gettelman (2008), A new two-moment bulk stratiform cloud microphysics scheme in the Community Atmosphere Model, Version 3 (CAM3). Part I: Description and numerical tests, *J. Climate*, *21*, doi:10.1175/2008JCLI2105.1.

Mote, P. W., K. H. Rosenlof, M. E. McIntyre, E. S. Carr, J. C. Gille, J. R. Holton, J. S. Kinnersley, H. C. Pumphrey, J. M. Russell III, and J. W. Waters (1996), An atmospheric tape recorder: The imprint of tropical tropopause temperatures on stratospheric water vapor, *J. Geophys. Res.*, *101*(D2), 3989–4006, doi:10.1029/95JD03422.

Murphy, D. M., and T. Koop (2005), Review of the vapour pressures of ice and supercooled water for atmospheric applications, *Q. J. Roy. Meteorol. Soc.*, *131*, doi:10.1256/qj.04.94.

Neale, R. B., et al. (2010a), Description of the NCAR Community Atmosphere Model (CAM 4.0), NCAR Technical Note, NCAR/TN-485+STR.

Neale, R. B., et al. (2010b), Description of the NCAR Community Atmosphere Model (CAM 5.0), NCAR Technical Note, NCAR/TN-486+STR.

Pfister, L., et al. (2001), Aircraft observations of thin cirrus clouds near the tropical tropopause, *J. Geophys. Res.*, *106*, 9765–9786.

Randel, W. J., and E. J. Jensen (2013), Physical processes in the tropical tropopause layer and their roles in a changing climate, *Nat. Geosci.*, *6*, 169–176, doi:10.1038/NGEO1733.

Rasch, P. J., and J. E. Kristjansson (1998), A comparison of the CCM3 model climate using diagnosed and predicted condensate parameterizations, *J. Climate*, *11*, 1587–1614.

Rienecker, M. M., et al. (2008), The GEOS-5 Data Assimilation System—Documentation of Versions 5.0.1, 5.1.0, and 5.2.0. Technical Report Series on Global Modeling and Data Assimilation, 27.

Riihimaki, L. D., and S. A. McFarlane (2010), Frequency and morphology of tropical tropopause layer cirrus from CALIPSO observations: Are isolated cirrus different from those connected to deep convection?, *J. Geophys. Res.*, *115*, D18201, doi:10.1029/2009JD013133.

Sassen, K., S. Matrosov, and J. Campbell (2007), CloudSat spaceborne 94 GHz radar bright bands in the melting layer: An attenuation-driven upside-down lidar analog, *Geophys. Res. Lett.*, *34*, L16818, doi:10.1029/2007GL030291.

Schiffer, R. A., and W. B. Rossow (1983), The International Satellite Cloud Climatology Project (ISCCP): The first project of the World Climate Research Programme, *Bull. Am. Meteorol. Soc.*, *64*, 779–784.

Schmitt, C. G., and A. J. Heymsfield (2009), The size distribution and mass weighted terminal velocity of low-latiude tropopause cirrus crystal populations, *J. Atmos. Sci.*, *66*, doi:10.1175/2009JAS3004.1.

Schwartz, M. J., et al. (2008), Validation of the Aura Microwave Limb Sounder temperature and geopotential height measurements, *J. Geophys. Res.*, *113*, D15S11, doi:10.1029/2007JD008783.

Song, X., G. J. Zhang, and J.-L. F. Li (2012), Evaluation of microphysics parameterization for convective clouds in the NCAR Community Atmosphere Model CAM5, *J. Climate*, *25*, doi:10.1175/JCLI-D-11-00563.1.

Stephens, G. L., and D. G. Vane (2007), Cloud remote sensing from space in the era of the A-Train, *J. Appl. Remote Sens.*, doi:10.1117/1.2709703.

Stephens, G. L., et al. (2008), CloudSat mission: Performance and early science after the first year of operation, *J. Geophys. Res.*, *113*, D00A18, doi:10.1029/2008JD009982.

Tabazadeh, A., S. T. Martin, and J. S. Lin (2000), The effect of particle size and nitric acid uptake on the homogeneous freezing of aqueous sulfuric acid particles, *Geophys. Res. Lett.*, *27*, 1111–1114.

Thompson, A. M., J. C. Witte, H. G. J. Smit, S. J. Oltmans, B. J. Johnson, V. W. J. H. Kirchhoff, and F. J. Schmidlin (2007), Southern Hemisphere Additional Ozonesondes (SHADOZ) 1998–2004 tropical ozone climatology: 3. Instrumentation, station-to-station variability, and evaluation with simulated flight profiles, *J. Geophys. Res.*, *112*, D03304, doi:10.1029/2005JD007042.

Tilmes, S., et al. (2012), Technical note: Ozonesonde climatology between 1995 and 2011: Description, evaluation and applications, *Atmos. Chem. Phys.*, *12*, 7475–7497.

Toon, O. B., R. P. Turco, D. Westphal, R. Malone, and M. S. Liu (1988), A multidimensional model for aerosols: Description of computational analogs, *J. Atmos. Sci.*, *45*(15), 2123–2143.

Turco, R. P., P. Hamill, O. B. Toon, R. C. Whitten, and C. S. Kiang (1979), One dimensional model describing aerosol formation and evolution in the stratosphere: I. Physical processes and mathematical analogs, *J. Atmos. Sci.*, *36*(4), 699–717.

Waliser, D., et al. (2009), Cloud ice: A climate model challenge with signs and expectations of progress, *J. Geophys. Res.*, *114*, D00A21, doi:10.1029/2008JD010015.

Walters, J. W., et al. (2006), The Earth Observing System Microwave Limb Sounder (EOS MLS) on the Aura Satellite, *IEEE Trans. Geosci. Remote Sens.*, *44*(5), 1075–1092.

Wielicki, B. A., B. R. Barkstrom, E. F. Harrison, R. B. Lee III, G. L. Smith, and J. E. Cooper (1996), Clouds and the Earth's Radiant Energy System (CERES): An Earth observing system experiment, *Bull. Am. Meteorol. Soc.*, *77*, 853–868.

Wilson, D. R., and S. P. Ballard (1999), A microphysically based precipitation scheme for the UK Meteorological Office Unified Model, *Q. J. Roy. Meteorol. Soc.*, *125*, 1607–1636.

Winker, D. M., M. A. Vaughan, A. H. Omar, Y. Hu, K. A. Powell, Z. Liu, W. H. Hunt, and S. A. Young (2009), Overview of the CALIPSO mission and CALIOP data processing algorithms, *J. Atmos. Oceanic Tech.*, *26*, 2310–2323.